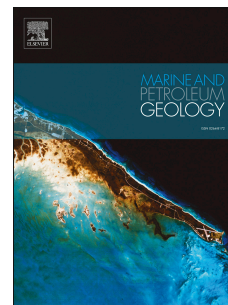


Journal Pre-proof

Contourite porosity, grain size and reservoir characteristics

Xiaohang Yu, Dorrik Stow, Zeinab Smillie, Ibimina Esentia, Rachel Brackenridge, Xinong Xie, Shereef Bankole, Emmanuelle Ducassou, Estefania Llave



PII: S0264-8172(20)30175-6

DOI: <https://doi.org/10.1016/j.marpetgeo.2020.104392>

Reference: JMPG 104392

To appear in: *Marine and Petroleum Geology*

Received Date: 14 January 2020

Revised Date: 2 April 2020

Accepted Date: 7 April 2020

Please cite this article as: Yu, X., Stow, D., Smillie, Z., Esentia, I., Brackenridge, R., Xie, X., Bankole, S., Ducassou, E., Llave, E., Contourite porosity, grain size and reservoir characteristics, *Marine and Petroleum Geology* (2020), doi: <https://doi.org/10.1016/j.marpetgeo.2020.104392>.

This is a PDF file of an article that has undergone enhancements after acceptance, such as the addition of a cover page and metadata, and formatting for readability, but it is not yet the definitive version of record. This version will undergo additional copyediting, typesetting and review before it is published in its final form, but we are providing this version to give early visibility of the article. Please note that, during the production process, errors may be discovered which could affect the content, and all legal disclaimers that apply to the journal pertain.

© 2020 Published by Elsevier Ltd.

CREDIT AUTHOR STATEMENT

All authors have played an important part in different parts of the research and/or writing, as follows:

Xiaohang Yu – principal author, all aspects

Dorrik Stow – principal author, all aspects

Zeinab Smillie – principal author, all aspects

Ibimina Esentia – grain size compilation and interpretation

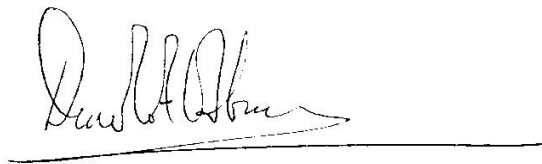
Rachel Brackenridge – grain size compilation and interpretation, previous grain size data

Xinong Xie – supervision of Yu, contribution to discussion

Shereef Bankole – provision of grain size data and manipulation

Emmanuelle Ducassou – all grain size analyses

Estefania Llave – all porosity data analyses

**Professor Dorrik Stow FRSE**

Professor of Geoscience, Institute of Geo-Energy Engineering

Heriot-Watt University, Edinburgh EH14 4AS, Scotland, UK

Email: d.stow@hw.ac.uk *Tel:* +44 (0)131 451 3138 *Mobile:* +44 (0)7 887 870 309



UK | DUBAI | MALAYSIA



*Celebrating our
Royal Charter*

Contourite Porosity, Grain Size and Reservoir Characteristics

Xiaohang Yu^a, Dorrik Stow^{b,a*}, Zeinab Smillie^b, Ibimina Esentia^b, Rachel Brackenridge^b, Xinong Xie^a, Shereef Bankole^b, Emmanuelle Ducassou^c, Estefania Llave^d

^a *College of Marine Science and Technology, China University of Geosciences, Wuhan, China*

^b *Institute of Geo-Energy Engineering, School of Energy, Geoscience, Infrastructure & Society, Heriot-Watt University, Edinburgh, EH14 4AS, UK*

^c *Department of Oceanography, Bordeaux University, Bordeaux, France*

^d *Instituto Geológico y Minero de España, Rios Rosas 23, 28003 Madrid, Spain*

* *Corresponding author*

Abstract

Contourites are now recognised as having a significant potential as hydrocarbon reservoirs in the subsurface, and several fields have been interpreted as comprising bottom-current reworked turbidite sands. However, very little has been published on the porosity characteristics of contourites. This study documents porosity data from IODP Expedition 339 sites in the Gulf of Cadiz. We use grain size analyses, porosity-depth plots and exponential models to yield a better understanding of grain size characteristics and facies, porosity characteristics, and the reservoir potential of contourites in the subsurface.

New grain size data for over 350 samples from the Cadiz contourites is presented, building on earlier work. These data confirm the distinctive trends in textural properties linked to depositional processes under the action of bottom currents. The finest muddy contourites (<20 microns) show normal grain size distributions, poor to very poor sorting becoming better with decreasing grain size, and zero or low skewness. These are contourite-hemipelagite hybrids. Muddy to fine sandy

27 contourites (20 to 200 microns) trend towards better sorting and initially fine-tail and
28 then coarse-tail skew. These represent typical depositional trends for contourites,
29 affected by current capacity and then increased winnowing at higher current speed.
30 Clean sandy contourites (around 200 microns) are the best sorted. Medium and
31 coarser-grained contourites show a trend towards poorer sorting. They result from the
32 action of dominant bedload transport, extensive winnowing, and mixed sediment
33 supply.

34 Porosity-depth relationships from four Cadiz sites show a moderately high initial
35 porosity for both sand and mud facies (50-60%) and a systematic decrease with depth
36 to around 35-40% near 500 m burial depth. According to the exponential models of
37 porosity with depth, contourite porosity should exceed 10% at 2500 m burial depth.
38 We compare the data from the Gulf of Cadiz Contourite Depositional System, with
39 those of the Eirik Drift, Newfoundland Drift, Gardar Drift and Canterbury Slope
40 Drifts. Similar depth trends are observed, and all show anomalies linked to
41 interbedded sandy and muddy facies, composition (carbonate vs siliciclastic), and the
42 presence of hiatuses in the sediment record.

43 These data provide good insight into the likely reservoir characteristics of
44 contourites, for both conventional and unconventional reservoirs. They are
45 comparable with those of existing contourite fields, most of which are mixed
46 turbidite-contourite systems.

47

48 **Keywords:** Contourites, porosity-depth trends, grain size characteristics, reservoir
49 characteristics

50 1. Introduction

51 Contourites are deep-water sediments deposited or substantially reworked by
52 bottom currents. They are commonly interbedded with other deep-water facies due to
53 the interaction of different kinds of currents (Rebesco and Camerlenghi, 2008). Since
54 Hollister and Heezen (1972) first defined the concept of contourites, the

55 understanding of these sediments has increased considerably, mainly focused on
56 sedimentary characteristics, facies models, and controlling factors (Faugères and Stow,
57 1993; Viana et al., 1998 ; Stow and Mayall, 2000; Stow et al., 2002b; Rebesco and
58 Camerlenghi, 2008; Stow and Faugères, 2008; Rebesco et al., 2014;). Contourite
59 drifts are widely distributed around the world (Rebesco and Camerlenghi, 2008; Chen
60 et al. 2014; Rebesco et al., 2014; Wen et al., 2016), and are recognised as providing
61 significant opportunity for future petroleum exploration (Stow and Mayall, 2000;
62 Pettingill and Weimer, 2002; Viana et al., 2007; Shanmugam, 2012). Recent research
63 on sandy contourite systems, such as the Cadiz sand sheet (Stow et al., 2013b),
64 Falkland sand sheet (Nicholson and Stow, 2019), Faroe–Shetland Channel (Masson et
65 al., 2010), and Riffian Corridor contourite sands (Capella et al., 2017), combined with
66 better understanding of unconventional reservoirs, have re-invigorated research into
67 the economic value of contourites. However, much work is still needed to better
68 characterise contourites as potential reservoirs, including their texture, porosity and
69 permeability attributes (Viana et al., 2007; Brackenridge et al., 2018;).

70 This paper focuses in particular on the grain size and porosity of contourites,
71 presenting new data from the Gulf of Cadiz contourite depositional system, offshore
72 Spain, derived from four sites (U1386, U1387, U1388 and U1389) of the International
73 Ocean Drilling Program (IODP) Expedition 339. These are combined with grain-size
74 data from CONTOURIBER sites (BC05, PC04, PC06 and PC08) as published by
75 Brackenridge et al.(2018) (Fig.1). We also access porosity data from four other IODP
76 sites for comparison, on Newfoundland drift, Eirik drift, Gardar drift and Canterbury
77 slope. In summary, the aims of this paper are as follows:

- 78 1) To discuss new grain size data from Cadiz contourites and so develop our
79 understanding of contourite depositional processes and their potential as
80 hydrocarbon reservoirs.
- 81 2) To present porosity-depth relationships for both the Cadiz contourites and
82 comparative drift systems, and to use exponential models for evaluating the
83 potential porosities at reservoir depths.

84 3) To consider these data in terms of the reservoir characteristics of contourites.

85 2. Methods and Database

86 2.1. Site data

87 The large Contourite Depositional System (CDS) of Gulf of Cadiz was deposited
88 under the influence of warm, high-salinity Mediterranean Outflow Water from
89 Pliocene to Recent (Fig.1). It is now well established as one of the prime contourite
90 depositional laboratories in the world (Maldonado et al., 1999; Stow et al., 2013b;
91 Hernández-Molina et al., 2016a;).

92 Five sites were drilled during IODP Expedition 339 in the Gulf of Cadiz CDS, at
93 between 570-1100 m water depths. These recovered a total of 4.5 km of core material
94 using the advanced piston corer system, the extended core barrel system, and the
95 rotary core barrel system (Stow et al., 2013a; Stow et al., 2014). This study mainly
96 focuses on geological data and core data (sediments and physical properties) from
97 four of these sites: U1386, U1387, U1388 and U1389. We further present
98 porosity-depth data derived from four other expeditions that drilled contourite systems,
99 namely IODP 303 site 1305, IODP 317 site 1352, IODP 342 site U1410, and IODP
100 303 site 1304 (Channell et al., 2006; Fulthorpe et al., 2011; Norris et al., 2014). This
101 database is summarised in Table 1.

102

103 Table.1 Data summary of site U1386, site U1387, site U1388, site U1389 of
104 IODP 339, site U1305 of IODP 303, site U1304 of IODP 303site, U1352 of IODP
105 317 and site U13410 of IODP 342 (Channell et al., 2006; Fulthorpe et al., 2011; Stow
106 et al., 2013a;Norris et al., 2014).

Expedition	Site	Number of holes	Distance between adjacent	Lat/long	Water depth (m)	Drift name	Total core recovery	Porosity sample amount
------------	------	--------------------	---------------------------------	----------	-----------------------	---------------	---------------------------	------------------------------

			holes (m)				(m)	
IODP 339	U1386	3	20	36°49.685'N; 7°45.321'W	561	CDS of Gulf of Cadiz	850.64	197
IODP 339	U1387	3	20	36°48.3210'; 7°43.1321'W	559	CDS of Gulf of Cadiz	1084.95	213
IODP 339	U1388	3	20	36°16.142'N; 6°47.648'W	663	CDS of Gulf of Cadiz	121	47
IODP 339	U1389	5	20	36°25.515'N; 7°16.683'W	644	CDS of Gulf of Cadiz	1123.5	200
IODP 303	U1305	3	20	57°28.5066'; 48°31.8132'W	3459	Eirik Drift	867.13	31
IODP 303	U1304	4	20	53° 3.4007' N; 33° 31.7814' W	3024	Gardar Drift	251.37	50
IODP 342	U1410	3	20	41°19.6993'N; 49°10.1847'W	3387	Newfoun dland Drift	748.8	143
IODP 317	U1352	4	20	44°56.2440'S; 172°1.3615'E	344	Canterbu ry Slope Drift	1443.65	1268

108 **2.2. Facies and Porosity data**

109 Sediment facies and their interpretation are well known for the Cadiz sites, as
110 they have been extensively studied by several of the present authors (Stow et al.,
111 2013b; Hernandez-Molina et al., 2014; Alonso et al., 2016; Hernández-Molina et al.,
112 2016a; Brackenridge et al., 2018). One of us (Dorrik Stow) has further examined
113 cores from each of the other four sites used in this study, and concurs with shipboard
114 scientists in their interpretation of mainly contourite, pelagite and hemipelagite
115 sedimentation.

116 Porosity data was measured by determination of moisture and density method
117 (Stow et al., 2013a) on discrete sediment samples. The working halves divided from
118 whole-round cores were used for taking discrete samples to determine the porosity.
119 About 10 cm³ samples from soft sediments were collected by a plastic syringe and
120 sampled every other section per core at the 59–60 cm position. Dry sample volume
121 was measured by a hexapycnometer system of a six-celled, custom-configured
122 Micromeritics AccuPyc 1330TC helium-displacement pycnometer. The measurement
123 focuses on the principal lithology of a section, and avoids small interlayers of different
124 grain size. Porosity (ϕ) data is calculated as $\phi = V_{pw}/V_{wet}$. The determination procedures
125 of these physical properties refer to the American Society for Testing and Materials
126 (ASTM) designation (D) 2216 (ASTM International, 1990). The porosity data used in
127 this study from each of the four other IODP sites was also measured and calculated by
128 the discrete moisture and density measurement technique (Channell et al., 2006;
129 Fulthorpe et al., 2011; Norris et al., 2014).

130 **2.3. Grain Size Analysis**

131 For this study, a total of 350 samples were analysed for grain size at the
132 University of Bordeaux, with a Malvern Laser Particle Size Analyser, following the
133 procedures used by Brackenridge et al (2018) in their recent exposition of contourite
134 textural characteristics. This measured grain sizes from 0.05 μm to 700 μm . The
135 standard procedure for grain size analysis in laser counters was used (McCave et al.,
136 1986; Cooper, 1998; Martins, 2003). Distributions are given in a geometric (volume)

137 scaling rather than arithmetic (number) scale to ensure there is equal emphasis on
138 changes in clay, silt and sand content in the histogram (Blott and Pye, 2001). All
139 analysis was carried out in the software GRADISTAT (Blott and Pye, 2001) using the
140 geometric graphical method as laid out by Folk and Ward (1957) to ensure that each
141 set of analysis can be directly compared to others in the study. Key statistical
142 measures include: mean, sorting (standard deviation), skewness, and kurtosis. The
143 formulae used for these measurements and the cut-off values for defining the sorting,
144 skewness and kurtosis are outlined in Blott and Pye (2001). After calculation of the
145 essential statistics, data were compared using cross plots (Folk and Robles, 1964;
146 Martins, 2003); the sediment classes are as defined by Wentworth (1922).

147 **3. Results**

148 **3.1. Sediment Facies and Distribution: Gulf of Cadiz**

149 The principal sediment facies recovered from the IODP drilling (Stow et al.,
150 2013a) throughout the six sites on the Cadiz Contourite Depositional System include
151 muds, silts and muddy sands. These are primarily siliciclastic in composition with a
152 minor to common (5-30%) calcareous biogenic fraction. Minor facies include: muddy
153 calcareous sediments (>50% CaCO₃) and foram-nannofossil ooze, which occur solely
154 within the Miocene succession at Sites U1386 and U1387; dolomitic mudstone and
155 dolostone, which occur locally at two sites (U1387 and U1391) within the early
156 Pliocene; and clean sandstone beds and chaotic clast-rich units, within the early
157 Quaternary and Pliocene at Sites U1386 and U1387.

158 These facies have been well documented in previous publications
159 (e.g. Hernández-Molina, 2016a) and have been interpreted in terms of depositional
160 processes as contourites, turbidites, reworked turbidites, debrites and slump deposits,
161 pelagites and hemipelagites (Stow et al., 2013b; Alonso et al., 2016;
162 Hernandez-Molina et al., 2016a) (Figs. 2 and 3). We are very confident of these
163 interpretations, which are based on multiple criteria at different scales of observation:
164 small-scale sedimentary characteristics (structures, textures, composition, fabric),

165 medium-scale seismic features (drifts, moats, seismic facies, widespread hiatuses),
166 and the large-scale geological and oceanographic setting.

167 Contourites are the dominant sediment type at the six CDS sites (U1386-U1391),
168 making up the 95% of the Quaternary and about 50% of the recovered Pliocene
169 succession. This facies group includes sand-rich, muddy sand, silty-mud and mud-rich
170 contourites, all of which were deposited at moderate (20-30 cm/ka to very high (> 100
171 cm/ka) rates of sedimentation. Clean, well-cemented sands are common in the
172 lowermost 20-40 m of the Quaternary succession at site U1386 and also present in the
173 same stratigraphic interval at site U1387. These are interpreted as bottom-current
174 reworked turbidites.

175 Below a marked hiatus at three of the CDS sites (U1386, U1387 and U1391), there
176 is clear evidence for more common downslope sedimentation within the Pliocene.
177 This dominates the succession older than about 4 Ma to the base of the Pliocene, but
178 also occurs interbedded with contourites younger than around 4.2 Ma. The downslope
179 facies are characterized by a mixed and exotic composition that includes shelf-derived,
180 fragmented macrofossils and benthic microfossils, as well as some glauconite and a
181 higher proportion of opaque heavy minerals and lithic grains. The turbidites show
182 clear normal grading from sand to mud above a sharp, erosive base, but mostly lack
183 other sedimentary structures, except for some with parallel lamination. Debrites are
184 chaotic, with contorted slump folds, isolated large clasts, and common shell debris in
185 a sandy, muddy matrix.

186 The porosity and grain size data presented below are all from the contourite facies.
187 These sediments are remarkably uniform in their mixed siliciclastic-biogenic
188 composition and textural attributes. They have a general absence of primary
189 sedimentary structures, except for a somewhat discontinuous and widely-spaced silt
190 lamination within muddy contourites that show the highest rates of sedimentation
191 (Site U1390). There is an intense, continuous bioturbation throughout with a
192 distinctive, small-scale, monotonous ichnofacies and local omission surfaces. Most
193 sections are characterized by bi-gradational sequences from inverse to normal grading,
194 but also include a range of partial sequences of which the base-cut-out sequences are

195 most common (Fig. 3). All these features are fully consistent with the established
196 facies model for fine and medium-grained contourites (Stow et al., 2002b; Stow and
197 Faugères, 2008).

198 Spatial distribution of the contourite elements along the Cadiz continental margin
199 are closely linked with the decrease in bottom-current speed down-flow from the exit
200 of the Gibraltar Gateway (Stow et al., 2013b; Hernandez-Molina et al., 2014;
201 Hernandez-Molina et al.2016b). The rocky substrate west of Gibraltar gives way to an
202 extensive contourite sand sheet, which extends along a mid-slope terrace for
203 approximately 100 km before diverging into several contourite channels around the
204 prominent seafloor relief created by mud volcanoes and diapiric ridges. Seismic data
205 and one industry borehole (Buitrago et al., 2001) indicate that this sand sheet is at
206 least 800 m thick. Site U1388 penetrated 220 m of this proximal sand sheet, before
207 the hole became too unstable to continue, and recovered rapidly-deposited, late
208 Quaternary, sandy contourites. The areal extent and vertical thickness of these clean
209 contourite sands display ideal reservoir characteristics, were they to be more deeply
210 buried, and are therefore especially significant for the oil and gas industry.

211

212 **3.2. Grain-Size Characteristics**

213 The 350 new grain size analyses presented here are all from contourites
214 recovered in four of the IODP 339 wells (U1386, U1387, U1388 and U1389). These
215 are plotted together with the 675 analyses of box core and piston core samples (BC05,
216 PC08, PC04, PC06) previously recorded by Brackenridge et al (2018), thereby
217 yielding the largest contourite grain-size set yet published (Fig. 4). The grain size
218 parameters measured – mean size, sorting, skewness and kurtosis – are presented as
219 cross-plots of mean-size vs sorting (Fig 4A), mean-size vs skewness (Fig 4B), and
220 mean size vs kurtosis (Fig 4C).

221 The data show a wide range of values in all the measured parameters. Mean
222 grain size ranges from clay to coarse sand (2 μm to 1200 μm , or 9 phi to 0 phi),
223 standard deviation (i.e. sorting) from very well sorted to very poorly sorted (σ 0.45 to

224 3.06 phi), skewness from very fine skew to very coarse skew (+0.7 to -0.6 phi), and
225 kurtosis from very platykurtic to very leptokurtic (0.5 to 2.6 phi). Grain-size of the
226 sediment cores PC04, PC08, U1386, U1387 and U1389 are mainly from clay to very
227 coarse silt, whereas parts of cores PC06 and U1388 contain much more sand, and core
228 BC05 is mostly dominated by fine to coarse sand. Overall, fine to coarse sands have
229 better sorting than clay and silt grain sizes.

230 Each of the different cross-plots shown (Fig.4) reveals a more or less sinusoidal
231 variation of parameters. The best sorted sediments are fine and very fine sand in
232 U1388 and PC06, whereas the least well sorted are very coarse silt in cores U1386,
233 U1387, U1388 and U1389. The sinusoidal trend (Fig. 4A) shows a decrease in sorting
234 from clay to coarse silt (9 to 5.5 phi), an increase from coarse silt to fine sand (5.5 to
235 2.5 phi), and a decrease from fine sand to coarse sand (2.5 to 0 phi). However, the
236 trend is not everywhere so well-defined. The coarser grain sizes show more scattered
237 sorting, as do the mean grain-sizes from ~6.5 phi to ~4.5 phi and σ value from
238 ~3.05 to ~2.3. Part of this scatter is due to slightly different trends at different sites.

239 The mean-size vs skewness sinusoidal curve (Fig. 4B) is offset from the
240 mean-size vs sorting curve. Skewness defines the symmetry of the grain-size
241 distribution curve, such that the skewness value of a normal distribution is 0. The
242 lowest values (coarse and very coarse skew, -0.6) are at around 6.5 and 1.5 phi, with
243 high values (very fine skew, +0.7) around 4 phi. Most of data points lie between
244 grain-sizes of ~7.5 to 6 phi (fine to coarse silt) and skewness between ~0.1 to -0.2.
245 Sediments with the finest skewness are very coarse silt to very fine sand, whereas
246 medium and coarse sand has the coarsest skewness. Most of the normal distributions
247 with very low or zero skew are observed in very fine silt to coarse silt sediments, and
248 a very few can be found in fine sands.

249 The plot of mean grain-size versus kurtosis (Fig. 4C) is less clearly sinusoidal.
250 Kurtosis defines the degree of peakedness of the distribution curve, more concentrated
251 if they have leptokurtic distribution, and more dispersed if they have platykurtic
252 distribution. The finer grained sediment, clay to coarse silt (9 to 4.5 phi), are mainly

253 mesokurtic and platykurtic, with the lowest values at around 5.5 to 4.5 phi. From
254 coarse silt to fine sand (4.5 to 3 phi), sediments show a rapid change from platykurtic
255 to very leptokurtic, and then a marked decline from fine to coarse sand (3 to 0 phi) to
256 very platykurtic distributions.

257 Plots of sorting versus skewness and kurtosis versus skewness are also shown in
258 Figure 4D and 4E, with the data points arranged in grain size classes rather than by
259 site. These relationships are quite complex, but do serve to illustrate at least three
260 distinct grain-size clusters with an elongate trend: (a) clay to fine silt (purple, black and
261 dark grey points) with poor to very poor sorting (1.5 – 2.5 phi), zero to low skewness
262 (+0.2 – -0.2 phi), and platykurtic distribution; (b) medium silt to fine sand (light grey
263 and green points) with very poor to good sorting (2.75 – 0.5 phi), zero to coarse-tail
264 skew (0 – -0.6 phi), and very platykurtic to leptokurtic distribution (0.6 – 2.5 phi); and
265 (c) medium to coarse sand (dark green and pink points) with poor to good sorting (1.5
266 – 0.5 phi), zero to very coarse-tail skew (0 – -0.7 phi), and platykurtic to leptokurtic
267 distribution (0.6 – 2.5 phi).

268 **3.3 Porosity Profiles**

269 We first present porosity-depth curves for the four Gulf of Cadiz wells (Fig. 5),
270 and then selected data from other contourite drift systems for comparison (Fig. 6).

271 **3.3.1 Gulf of Cadiz Contourites**

272 The porosity-depth profile at site U1386 is shown in Figure 5. The sediments
273 above 420 m depth are exclusively contourites, whereas below this they become
274 interbedded with turbidites. According to this profile, the overall porosity range is
275 between 34-58% (with three outlier data points), and slowly decreases from ~50-60%
276 at the top to ~40-45% at the base of the well. The data points appear more scattered
277 below 300 m, which corresponds to the beginning of slight and dispersed cementation.
278 Although there are relatively few sandy contourites present, we can discern different
279 sub-trends for muddy and sandy contourites as indicated by the yellow and green
280 trend lines, respectively. The porosity of muddy contourites gradually decreases in the

281 first ~170 m, and then increases slightly before decreasing again with a faster rate up
282 to a depth of ~270 m. There is little further change below ~270 m so that the average
283 porosity of mud remains at ~40-45%.

284 The trend line of porosity with depth for silty sands (based on five data points)
285 shows a decrease from 45% at 20 m depth to around 35% at over 400 m depth. The
286 sands and sandy silts below 400 m are somewhat anomalous, with porosity values of
287 40-50%.

288 The porosity profile of site U1387 is shown in Figure 5. Contourites are the
289 principal facies above ~460 m, after which they are interbedded with turbidites and
290 related facies. The porosity-depth trend for contourites shows an overall porosity
291 between 37-58%, with three outlier points in sandy sediments, which are most likely
292 due to cementation (Stow et al., 2013a). The average porosity is ~50-60% at the top
293 and decreases to 40-45% at the bottom, with three sub-trends. Porosity data for sandy
294 contourites is insufficient to present any distinct trend. The porosity of mud
295 contourites reduces to ~44% at a depth of ~340 m, increases by approximately 4%
296 over the next ~110m interval, and then decreases again at a similar rate as the topmost
297 section. There are possible breaks in these trends at around 400 m and at 700 m.

298 The amount of porosity data gathered from site U1388 is much less than from the
299 other sites, due to the difficulty of core recovery within these coarser-grained
300 sediments (Stow et al 2013a). However, there are some interesting trends apparent in
301 the 250 m of section recovered (Fig. 5). The porosity lies between 38-52% for muddy
302 contourites and relatively lower, 42-48%, for sandy contourites. Both show an initial
303 decrease with depth ~150 m interval, and then a marked break in trend and slight
304 increase to 47%.

305 Overall range of porosity at site U1389 is mainly between 35-58%, as shown in
306 the porosity-depth profile, with 5 outlier points (Fig. 5). The porosity in three samples
307 near the top is 60-70%, but rapidly decreases to 45-55% at the depth of tens of meters,
308 and then gradually decreases to 35-45% at a depth of ~300 m. There is a distinct

309 break in trend associated with a minor hiatus at this depth, after which the values
310 jump higher by 4-5%, and then proceed to decrease from ~49% to ~43% at a similar
311 rate as the topmost interval. The very low value at around 500 m is due to
312 cementation, whereas the anomalously high value at 600 m has no clear explanation.
313 The trend in sandy contourite porosity values is from 55-38%, at a similar rate of
314 decrease to the muddy contourites.

315 **3.3.2 Other Contourite Porosity Profiles**

316 To compare the porosity characteristics of contourites from the Gulf of Cadiz
317 with those of different settings, we selected four sites from other IODP expeditions –
318 site U1305 (IODP 303) on the Eirik drift, site U1304 (IODP 303) on the Gardar drift,
319 site U1410 (IODP 342) on the Newfoundland drift, and site U1352 (IODP 317) on the
320 Canterbury slope. Sites U1410 and U1305 from the Newfoundland and Eirik drifts are
321 at significantly greater water depths, in excess of 3000 m, than those sites from the
322 Gulf of Cadiz, whereas water depth of site U1352 on the Canterbury slope is a little
323 shallower, but the depth of penetration below the seafloor is much greater – close to
324 2000 m burial depth (Table.1). Sediments of all these sites are less sandy than those of
325 IODP 339 and also generally more carbonate-rich (Channell et al., 2006; Fulthorpe et
326 al., 2011; Norris et al., 2014).

327 *Eirik Drift:* Site U1305 is located south of Greenland and drilled on the
328 south-western border of Eirik drift, which was generated by Norwegian Sea Overflow
329 Water during Pliocene and Quaternary (Channell et al., 2006). The sediments consist
330 of mixed terrigenous, biogenic and detrital carbonate material, deposited during
331 Pliocene to Pleistocene. At this site, the lithology is very uniform, predominantly silty
332 clay with a relatively small amount of nannofossil ooze and sandy clay, and no sandy
333 contourites. The majority of samples show porosities between 50% and 77% (Fig. 6),
334 with two notable outliers. The original porosity is relatively high (~74-77%), and
335 decreases with depth to around 50-53% at the bottom (~230 m depth). There is some
336 irregular oscillation apparent in this overall trend.

337 *Gardar Drift:* Site U1304 is located on the eastern flank of the Mid-Atlantic
338 Ridge, south of Iceland in the North Atlantic. Sediment recovery is from Late
339 Pliocene to Holocene, and consists of interbedded nannofossil ooze and diatom ooze
340 with silty clay (Channell et al., 2006). The porosity data points are relatively scattered
341 (Fig. 6). Range of overall data points is from 68% to 87% with one obvious outlier.
342 The original porosity is very high, around nearly 80%, and there is almost no marked
343 decrease to the bottom of the hole (~240 m depth).

344 *Newfoundland Drift:* Site U1410 is located on the Newfoundland ridge, North
345 Atlantic, and recovered sediments from the Paleogene-Recent Newfoundland drift
346 (Norris et al., 2014). It is divided into four different lithological units: Unit I (0-34 m)
347 is mixed clay sediments and foraminiferal ooze, Unit II (34-64 m) mainly has clay
348 sediments with some nannofossil ooze, Unit III (64-211 m) is dominated by clay and
349 nannofossil ooze, and Unit IV (211-258 m) predominantly chalk and claystone.
350 Overall, the porosity decreases from an average of 70-75% at the top to around 40-45%
351 at the bottom (Fig. 6). There is a marked porosity decrease by 10-15% in the first 50
352 m interval, and then there only a very slight decrease down to 170 m. The rapid
353 decrease from 170 m appears to be linked to compaction and early cementation of
354 clay and ooze resulting in the formation of claystone and chalk.

355 *Canterbury Slope:* Site U1352 is located on the upper slope of Canterbury
356 Bight, New Zealand, and recorded sediments deposited during late Eocene to early
357 Oligocene (Fulthorpe et al., 2011). It is divided into three main lithological units,
358 which mainly consist of interbedded clay and mud, sandy mud, muddy sand. There is
359 more siliciclastic content in the upper part and more carbonate in the lower part. The
360 three lithological units are: Unit I (0-11 m) is dominated by mud-rich sediments and
361 interbedded sand; Unit II (711–1853 m) mainly consists of uncemented sandy mud
362 and cemented sandy marlstone; and Unit III (1853–1924 m) consists of cemented
363 sandy and silty limestone. The porosity-depth profile is relatively more marked at this
364 site because of the relatively deeper burial depth compared with contourites of the
365 other sites considered. The porosity range at the surface is ~40-56%, with one value

366 of 65%, whereas the average porosity at the base is 4-14% (Fig. 6). There is a modest
 367 decrease in porosity in the upper 500 m interval, but with the beginning of
 368 cementation from 500 m, the porosity points are more scattered, and the porosity
 369 decreases more rapidly from 40% to 25% in the next 400 m interval. Below that, the
 370 porosity gradually decreases with depth from 900-1850 m to around 4-14%.

371

372 **4.2. Exponential Models of the Porosity-Depth Relationship**

373 The porosity-depth relationship is the principal factor to be considered for
 374 evaluating the reservoir potential of any particular sedimentary succession or facies.
 375 Rubey and Hubbert (1959) established a general exponential equation for the
 376 porosity-depth relationship under normal pressures, which they formulated as:

$$377 \quad f = f_0 e^{-cz}$$

378 (where f =porosity at normal pressure, f_0 = original porosity, e = natural logarithm, c =
 379 compaction coefficient, z =depth)

380 Using this equation, Rubey and Hubbert (1959) analysed the porosity-depth
 381 exponential relationship of shale and mudstone, whereas Sclater and Christie (1980)
 382 found the exponential relationship for sandstone by studying North Sea reservoirs.
 383 The parameters from these previous studies can be used as the normal values for sand
 384 and mud (Table.2).

385 Table.2 Parameters for the normal exponential porosity-depth equation (Rubey and
 386 Hubbert, 1959; Sclater and Christie, 1980)

Lithology	Original porosity (f_0)	Compaction coefficient (c)
Sandstone	0.49	$0.27 \times 10^{-3} \text{ m}^{-1}$
Mudstone	0.63	$0.51 \times 10^{-3} \text{ m}^{-1}$

387

388 According to these previous studies, therefore, the exponential porosity-depth
 389 models can also be derived from porosity data of the study area as presented above.
 390 The parameters used in the exponential equations are presented in Table 3, showing
 391 values for mud and sand facies separately. Insufficient sandy contourite values from
 392 Site U1387 precludes developing the exponential equation in this case.

393 Table. 3 Parameters and exponential equations derived from IODP339 data

394 *Mud:*

Site	Original porosity(f_0)	Compaction coefficient (c)	Equation
U1386	0.4937	$0.4 \times 10^{-3} \text{ m}^{-1}$	$f=0.4937e^{-0.4 \times 10^{-3} z}$
U1387	0.4457	$0.2 \times 10^{-3} \text{ m}^{-1}$	$f=0.4457e^{-0.2 \times 10^{-3} z}$
U1388	0.4406	$0.6 \times 10^{-3} \text{ m}^{-1}$	$f=0.4406e^{-0.6 \times 10^{-3} z}$
U1389	0.4958	$0.3 \times 10^{-3} \text{ m}^{-1}$	$f=0.4958e^{-0.3 \times 10^{-3} z}$

395 *Sand:*

Site	Original porosity(f_0)	Compaction coefficient (c)	Equation
U1386	0.4716	$0.6 \times 10^{-3} \text{ m}^{-1}$	$f=0.4716e^{-0.6 \times 10^{-3} z}$
U1387	-----	-----	-----
U1388	0.4578	$0.4 \times 10^{-3} \text{ m}^{-1}$	$f=0.4578e^{-0.4 \times 10^{-3} z}$
U1389	0.4797	$0.5 \times 10^{-3} \text{ m}^{-1}$	$f=0.4797e^{-0.5 \times 10^{-3} z}$

396

397 Using these models, the exponential curves have been drawn and shown in
 398 comparison with the curves for mud and sand under normal compaction pressure.
 399 These show predicted trends of porosity change with depth for each of the Gulf of
 400 Cadiz sites (Fig.7). It should be noted that these curves simply provide an
 401 approximation of likely trends in porosity-depth curves, with predicted values
 402 extended to a depth of 2500m. Note that the porosity predictions are based solely on

403 the exponential equations derived from IODP 339 data. The actual values will be
404 subject to a range of more complicating variables, such as differential cementation,
405 long-duration hiatuses in the sediment record, and so on.

406 *Contourite muds:* The exponential curves of porosity for sites U1386 and U1389
407 each show trends comparable with that for normal mud. Due to the locally increasing
408 porosity intervals of U1387 and U1388, these curves indicate an increasing trend, so
409 that the exponential curves of these two sites are invalid. The original porosity (f_0) of
410 U1386 of around 50% is ~13% less than that of normal mud, but by reason of its
411 lower compaction coefficient, the rate of porosity decrease for U1386 is relatively
412 slower, so that by 2500 m depth, the predicted porosity of U1386 is very close to that
413 of normal mud - at about 18%. A similar result is apparent for site U1389, for which
414 the exponential model predicts a decrease from 50% at the surface to ~24% at 2500 m
415 depth, or about 6% higher than that for normal mud.

416 *Contourite sands:* With relatively less data points available (and none for
417 U1389), the exponential curves for contourite sand porosity are less robust. From a
418 surface porosity of between 45-55%, each of the three sites is predicted to decrease to
419 between 10-17% at 2500 m depth. These exponential porosity curves compare with
420 that for normal sand, which decreases from 49% to 25% at 2500 m.

421 **4. Discussion**

422 **4.1. Grain size of contourites**

423 Grain size parameters are one of the fundamental characteristics of sediments,
424 strongly linked with sedimentary environment, sediment supply, current energy and
425 depositional process. Sediment texture is also a key attribute for assessing the nature
426 of reservoirs and seals in the subsurface. There have been many hundreds of
427 publications on sediment textures over the past six decades, since some of the early
428 work that focussed largely on continental sedimentary environments (Folk and Ward,
429 1957; Mason and Folk, 1958; Martins, 1965; Pollack, 1961; Friedman, 1992).
430 Important syntheses of this work, including marine and deep marine environments,

431 are published in a number of key sedimentology texts (Blatt, 1992; Friedman, 1992;
432 Leeder, 1999; Stow, 2005; Bridge and Demicco, 2008; Boggs, 2009;). The strong link
433 between grain size and porosity-permeability characteristics is highlighted by Selley
434 (2000), and Gluyas and Swarbrick (2004), amongst others. However, there are still
435 relatively few papers documenting the grain-size characteristics of contourites and
436 almost none that are directly linked with reservoir potential (Stow and Holbrook,
437 1984; Stow and Faugères, 2008; Mulder et al., 2013; Brackenridge et al., 2018;).

438 This last paper (Brackenridge et al., 2018) is a particularly important synthesis of
439 grain-size data from the Gulf of Cadiz contourites, based mainly on gravity and box
440 core samples from near-surface sediments. We have incorporated these data with our
441 new grain-size analyses from the IODP wells, and the expanded cross-plots of
442 grain-size parameters clearly re-inforce the validity of relationships and sinusoidal
443 trends established previously. The new data points greatly extend information on clay
444 to coarse silt, and some very fine sand contourites. We further develop the
445 interpretation and discussion below, with reference to a simplified overlay of the three
446 cross plots – mean size vs sorting, mean size vs skewness, and mean size vs kurtosis
447 (Fig. 8A). Using the mean size vs sorting as a base, we define three main contourite
448 types as follows (Fig. 8B).

449 *Clay to fine silt contourites:* These very fine-grained contourites (mean 9 to 5.5
450 phi, 2-20 um) show a general poor to very poor sorting trend, low to zero skewness,
451 and a platykurtic distribution. These characteristics are compatible with deposition in
452 the absence of current control (i.e. hemipelagic deposition) to that beneath very weak
453 bottom currents (< 10 cm/s). Much of the material will have been transported as larger
454 flocs, so that the disaggregated grain-size character illustrated here is difficult to fully
455 interpret. The broad scatter of points as well as the clustered trends from individual
456 sites are most likely due to intensive bioturbational mixing, as well as to different
457 proportions of principal components, as suggested by the platykurtosis.

458 *Medium silt to fine sand contourites:* This range of contourite grain sizes (mean
459 5.5 to 2.25 phi, 20-200 um) are strongly influenced by bottom-current deposition and

460 winnowing. We refer to the distinctive trends of grain-size parameters (Fig. 8) as the
461 standard *contourite depositional trend*. These are from very poor to well-sorted, zero
462 to fine-tail to coarse-tail skewness, and from very platykurtic to leptokurtic. Overall,
463 sorting of coarser sediments is better than finer sediments. We concur with
464 Brackenridge et al. (2018) that the finer sediments within this range are mainly
465 deposited from suspended load, whereas the saltation load becomes progressively
466 more prevalent as the grain size increases from coarse silt to fine sand. The change
467 from fine-tail to coarse-tail skewness follows this trend, and indicates transition from
468 a deposit controlled principally by the maximum carrying capacity of the current
469 (10-20 cm/s), to one affected by progressive winnowing at higher current speeds
470 (15-25 cm/s).

471 *Medium and coarse sand contourites:* These purely sandy contourites (mean
472 2.25 to -0.5 phi, 200-1250 um) are strongly influenced by bottom current action. They
473 show a general trend in grain-size parameters, with some degree of scatter, from well
474 to poorly sorted, coarse and very coarse-tail skew to zero skew, and from mesokurtic
475 to platykurtic. Strong current winnowing, and grain saltation is augmented by
476 widespread bedload traction, which increases in importance with increase in
477 grain-size. The suspended load is swept downstream from the depositional site. The
478 greater scatter of data points in this sector is due to innate variability in current speed,
479 and a distinctly mixed supply of different source material, both siliciclastic and
480 bioclastic.

481 These interpretations of the different contourite grain-size classes are compatible
482 with work by previous authors (Allison and Ledbetter, 1982; Brunner, 1984; McCave,
483 1984; Viana et al., 1998; Faugères and Mulder, 2011; Alonso et al., 2016;
484 Brackenridge et al., 2018). Our three classes can be related to the contourite
485 end-member models proposed by Brackenridge et al. (2018) as follows: clay to fine
486 silts (model B), medium silt to fine sand (models C and D), and medium to coarse
487 sands (model A). The principal controls on these textural properties are: current speed,

488 sediment supply, flocculation, and bioturbation. We make a few further observations
489 on the first two of these controls.

490 *Current speed:* The link between contourite grain size and bottom-current speed
491 has long been recognised (Ledbetter and Ellwood, 1980; McCave, 1984; McCave,
492 2008), and is proposed as the principal control to explain the standard bi-gradational
493 sequence model for contourites (Gonthier et al., 1984; Stow et al., 2002b; Stow and
494 Faugères, 2008). The (de-carbonated) grain-size fraction between 10-63 μm , known
495 as *sortable silt (SS)*, is commonly used as a proxy for current speed (McCave et al.,
496 1995; McCave, 2008). However, the sortable silt size range currently used matches
497 only one trend on the mean size vs skewness (Fig. 8), whereas the distinctive
498 contourite depositional trend, which we identify in this paper from the grain-size vs
499 sorting cross-plot, is from 20-200 μm . We therefore propose that a new sortable silt
500 and sand proxy (SSS) should be developed to better reflect the full grain-size range
501 that is strongly controlled by current speed. Work is currently in progress on this
502 topic.

503 *Sediment supply:* The sediment source and supply route also have a significant
504 influence on grain-size properties. For contourite systems, there can be supply from
505 vertical settling of pelagic material, slow hemipelagic advection, lateral input from
506 turbidity currents, and directly from the bottom currents via local or more distant
507 seafloor erosion. Stow et al. (2008) attempt to constrain an overall sediment budget
508 from these different sources for a 'typical' contourite drift, but readily acknowledge
509 that different drifts and different parts of the same drift will receive material from
510 these sources in varying proportions.

511 For the Gulf of Cadiz contourites documented in this paper, we interpret the
512 broad scatter of data points as in part due to different sedimentary material from a
513 range of sources. This is especially true for the finest (clay-silt) and coarsest
514 (medium-coarse sand) contourites for which current speed is not the sole or principal
515 control on grain size. The locations of sites U1388, BC05, PC04, PC06 and PC08 are
516 much closer to Gibraltar gateway than U1386, U1387 and U1389 (Fig.1), and are

517 therefore affected by both different current speeds and different sediment supply.
518 Brackenridge et al. (2018) pointed out samples from PC04 and PC06 have parallel but
519 separated trends, which they interpret as sediment supplied to PC04 from the
520 Southern Channel, which transports sediments from the Gibraltar gateway and its
521 adjacent margins, and sediment supplied to PC06 mainly from downslope processes.
522 We note similar partial separation of trends for sites U1386, U1387 and U1389.

523 **4.2. Porosity-Depth Relationships**

524 For the Gulf of Cadiz contourites, both the actual data plots and the exponential
525 porosity-depth curves show some significant departures from the normal trends for
526 sand and mud, as proposed by Rubey and Hubbert (1959) and Sclater and Christie
527 (1980) under normal conditions of pressure. In particular, the Cadiz sites, (a) have
528 lower porosity values at the surface, and (b) show irregularities and breaks in the
529 porosity depth profiles. In general, porosity decrease is mainly dominated by the
530 mechanism of physical compaction above ~500 m burial depth, through which grain
531 rearrangement accommodates to the overlying pressure (Athy, 1930; Busch, 1989).
532 Below 500 m, porosity reduction takes place as a response to a combination of
533 compaction, cementation and dissolution.

534 There are several possible factors that may have led to the abnormal porosity
535 profiles for the Cadiz contourites. Firstly, the primary porosity of surface sediments
536 may be different where deposited under the persistent influence of bottom currents,
537 perhaps as a result of different sediment fabric. This might explain the lower than
538 normal surface porosity observed. Secondly, the parts of the depth profiles with
539 higher than expected porosity values suggest abnormal pressure or overpressure
540 conditions and hence the relative under-compaction of the sediments (Fig.9).

541 This condition can arise during sediment compaction where pore fluids cannot
542 readily escape or the fluid expulsion rate is very low (Osborne and Swarbrick, 1997;
543 Waples and Couples, 1998). High sedimentation rates (>10cm/ka) of fine-grained
544 sediment is known to lead to overpressure in many sedimentary basins in the world.

545 Sedimentation rates for the Cadiz sites certainly meet this criterion (Stow et al., 2013a)
546 – 15-35 cm/ka at U1386, 15-25 cm/ka at U1387, up to 60 cm/ka at U1388, and 30-40
547 cm/ka at site U1389.

548 Furthermore, dolomite cementation occurred just below the major hiatus at site
549 U1387, and is believed to be widespread across the drift system. If this is the case,
550 then it may act as a local seal and hence barrier to fluid expulsion and so generate
551 overpressure and decrease the porosity reduction (Wangen, 2010). Other locally
552 cemented or partially cemented zones may account for other areas of overpressure and
553 porosity anomaly. Certainly, overpressure is an efficient way to preserve porosity in
554 the subsurface (Jansa and Urrea, 1990; Stricker and Jones, 2018). Scherer (1987)
555 estimated porosity retention of nearly 2% for every 1000 psi overpressure in
556 sandstone reservoirs.

557 **4.3 Comparison of Porosity Profiles**

558 The porosity profiles of the Cadiz contourite sites are all quite similar, although
559 they each show some anomalous variation and distinct profile breaks (Fig. 10). The
560 sandy contourite site (U1388) has slightly lower porosity values on average.
561 Comparing these with the other contourite systems documented herein reveals further
562 interesting information. The two drift sites that are distinctly more biogenic in
563 composition (Newfoundland drift is carbonate-rich, Gardar drift is mixed
564 carbonate-siliceous biogenics) have significantly higher surface porosities than in
565 Cadiz (Fig. 10B and 10C). The Newfoundland site also undergoes relatively early
566 cementation, so that porosities decrease rapidly below about 170 m depth. The Eirik
567 drift site also has higher surface porosities, which then decrease quite rapidly (Fig.
568 10A). This site is located on a distal part of the drift and is also relatively
569 biogenic-rich in the upper 100 m. It seems evident that biogenic contourite systems
570 have higher primary depositional porosity than siliciclastic and mixed drifts, and are
571 then more prone to early and differential cementation.

572 By contrast, the Canterbury slope contourites have a similar siliciclastic
573 composition and show very similar surface porosities to those of Cadiz, as well as a
574 closely parallel trend of decrease, at least down to 860m depth (Fig.10D). Below that
575 depth, the Canterbury contourites are more carbonate-rich and become more subject
576 to variable cementation. All sites are characterised by some anomalous trends and
577 breaks in profile, which we suggest are typical of contourite systems, especially those
578 with widespread hiatuses and mud-rich or biogenic-rich composition.

579 **4.4 Reservoir Potential**

580 **4.4.1 Modern analogues**

581 There is considerable interest at present in contourites as potential reservoirs,
582 both conventional and unconventional, with some authors suggesting that they will be
583 at the forefront of deep-water exploration in the coming decades (Shanmugam, 2006;
584 Viana, 2008; Stow et al., 2011; Shanmugam, 2012; Hernández-Molina et al., 2016b;
585 Stow et al., 2013b). Recent studies have documented the presence and widespread
586 extent of contourite sand sheets in slope settings. These include siliciclastic examples
587 in the Gulf of Cadiz (Buitrago et al., 2001; Stow et al., 2013b; Brackenridge et al.,
588 2018), Hebridean margin (Stow et al., 2002a), and on the Falkland slope (Nicholson
589 and Stow, 2019), as well as biogenic carbonate examples on the Bahama Banks
590 (Shanmugam, 2017) and offshore the Maldives (Lüdmann et al., 2018; Lüdmann et al.,
591 2013). These modern analogues provide good information on contourite architecture,
592 showing extensive sand sheets covering 4,000-25,000 km² and with thicknesses from
593 a few tens of metres to several hundreds of metres. The sediment properties reveal
594 both clean sands and muddy bioturbated sands, interbedded with muddy contourite
595 intervals.

596 Most of the contourites documented in this study from the Gulf of Cadiz are fine
597 grained (muds and silts), although these are interbedded in parts, especially proximal
598 to the Gibraltar gateway, with sandy contourites. The very fine and medium sands
599 show the best sorting characteristics, with little clay matrix, and would offer the best
600 reservoir properties in terms of porosity and permeability when buried. These

601 well-sorted contourite sands have been subjected to active winnowing away of fine
602 silts and clays by moderately strong bottom currents. Coarse-grained sandy
603 contourites are slightly less well sorted, partly as a result of intermittent bedload
604 traction and partly due to a more mixed sediment supply. In some areas, this supply
605 was most likely from downslope turbidity currents.

606 The porosity measurements reported here from the Cadiz system record the
607 dominance of extensive muddy contourites, and rather less sandy contourites. Both
608 show slightly lower than normal porosities (typically 50-60%) in near-surface
609 sediments, which is around 10-15% lower than for 'normal' muds and sands. The
610 observed decrease in the first few hundreds of metres and the predicted values from
611 exponential porosity-depth curves for both muddy and sandy contourites indicate that
612 they are likely to preserve good porosity values at reservoir depths – 16% for sands
613 and 18-24% for muds at 2500 m burial depth. However, because of the commonly
614 interbedded nature of these facies, as well as the occurrence of widespread hiatuses in
615 contourite systems, the porosity-depth profiles are likely to show anomalies.
616 Over-pressured zones with higher than normal porosities were observed in the Cadiz
617 wells.

618 Comparison with porosity-depth profiles compiled from four other contourite
619 systems confirms the patterns observed in Cadiz in the case of the Canterbury slope
620 system, but also reveal some differences for bioclastic (carbonate and siliceous)
621 contourites. These have higher primary porosities at the surface, but then are more
622 subject to cementation and dissolution with depth of burial. All the contourite systems
623 examined here show that anomalous porosity-depth profiles are most likely the norm.

624 Whereas we do not have permeability measurements for the mainly
625 unconsolidated sediments presented in this study, we can use a standard
626 porosity-permeability cross plot for different grain sizes (Chilingar, 1964) in order to
627 infer likely permeabilities of our contourite sediments in the subsurface (Fig. 11).
628 Taking an average porosity of around 14% for sandy contourites and 20% for muddy
629 contourites (as predicted at 2500 m burial depth), permeabilities would be 100-1000

630 mD for sands and 30-150 mD for muds. These are respectable values for conventional
631 and unconventional reservoirs, respectively.

632 **4.4.1 Subsurface reservoirs**

633 Contourite reservoirs are beginning to be recognised in the subsurface, especially
634 those interpreted as bottom-current reworked turbidites. These include the upper parts
635 of the giant Marlim oilfield in the Campos Basin (Moraes et al., 2007; Mutti and
636 Carminatti, 2012), the Mzia and Coral super-giant gas fields off Mozambique
637 (Fonnesu et al., 2020; Intawong et al., 2019; Palermo et al., 2014; Sansom, 2018), the
638 Yinggehai basin and Baiyun sag in the northern South China Sea (Gong et al., 2016;
639 Huang et al., 2017), and the Snorre field on the Norwegian slope (Rundberg and
640 Eidvin, 2016). In the case of the Marlim field, the reworked facies are interpreted as
641 highly bioturbated fine to medium contourite sands, relatively more poorly sorted than
642 the associated turbidite sands with a muddy matrix. The porosity is typically 20~30%
643 and the permeability around tens of millidarcies, although some mud-rich intervals
644 with very low permeability form baffles or barriers. However, according to Moraes et
645 al. (2007), the contourites have good lateral continuity, and even those contourites
646 with bioturbation and cement still form good quality reservoir.

647 In the Santos basin, offshore Brazil, Mutti et al. (2014) interpret both
648 bottom-current reworked turbidite reservoirs and sandy contourite reservoirs with
649 little evidence of downslope supply, although Viana (2008) also notes the existence of
650 coarse-grained turbidites as the likely source of extensive redistribution by bottom
651 currents. Seismic attribute mapping from 3D seismic show a number of
652 morphological features attributed to bottom currents, including large abyssal sand
653 dunes, barchan dunes, sand ribbons, sand waves and furrows, all with an along-slope
654 orientation. These sandy contourites are mainly fine sands, well sorted with low clay
655 matrix, and show good primary porosity (over 35% in places) and high permeability.
656 They are laterally extensive and up to hundreds of meters in thickness.

657 In the study of Bein and Weiler (1976), parts of the Cretaceous Talme Yafe
658 Formation are described as including carbonate-rich contourites deposited on a
659 continental slope. This formation is over 3 km thick and covers a large area of the
660 Arabian Craton in Israel. The sediments mainly dominated by very fine to very
661 coarse-grained siliciclastics, but also include significant biochemical carbonate and
662 carbonate skeletal fragments. Deposition is interpreted as due to both gravity currents
663 and bottom currents. Some of the coarser sediments are believed to have been
664 supplied by bottom-current generated by storms. The Helez-Brur-Kokhaw oil field is
665 reservoired in the Talme Yafe Formation, with some of the production coming from
666 carbonate and mixed bioclastic-siliciclastic contourites (Bein and Sofer, 1987).

667 Unconventional reservoirs are now a hugely important and growing source of oil
668 and gas exploration and production worldwide. Generally, these reservoirs consist of
669 fine-grained sediment (mud and silt), have very low to low porosity values (below
670 10%), low to very low permeability (below 20 mD), and high total organic carbon
671 content (normally over 2 wt%) (Zhu et al., 2012; Benayad et al., 2013; Bruna et al.,
672 2013; Haris et al., 2017; Mahmood et al., 2018; Yang, 2018). Some authors have
673 suggested that the highly productive shale-gas reservoirs of the Interior Seaway in the
674 USA may be contourites in part (Viana, 2008). A similar interpretation has recently
675 been proposed for the Ordovician-Silurian Longmaxi shale-gas formation in China (Li
676 et al., 2016). We have reservations about both these interpretations, but further work
677 is required.

678 However, the data presented in this study does suggest that fine-grained
679 contourites have many of the characteristics that would make them good
680 unconventional reservoirs. The interbedding of more silt-rich and mud-rich layers, the
681 porosity-depth profiles, anomalies and over-pressured zones, as well as their great
682 thickness and lateral extent are all favourable attributes. We are currently studying the
683 total organic carbon (TOC) content and type for contourite systems globally, and
684 preliminary results show many with high values (> 2% TOC). Shipboard data from

685 the Cadiz contourites show 1-2% TOC for most of the muddy contourites, increasing
686 to 4% for some of the interbedded contourite-turbidite section (Stow et al., 2013a).

687

688 **5 Conclusions**

689 This study presents new grain-size data for contourites from the Gulf of Cadiz,
690 which has led to improved understanding of the contourite depositional process and
691 primary information for reservoir characterisation in the subsurface. Furthermore, it
692 presents contourite porosity data for the first time from four Cadiz sites and from four
693 other IODP contourite sites, for comparison. Porosity-depth profiles, and exponential
694 models for porosity prediction at reservoir depths, are considered in the light of
695 growing interest in the hydrocarbon prospectivity of contourites. The key findings of
696 significance are:

- 697 • Contourite facies can be considered according to their principal grain-size
698 properties. We recognise three main types, as follows.
- 699 • Clay to fine silt contourites (2-20 μm) show normal grain-size distributions, poor
700 to very poor sorting becoming better with decreasing grain size, and zero or low
701 skewness. These are deposited by settling from weak bottom currents with a very
702 fine suspension load and by hemipelagic settling – they are
703 contourite-hemipelagite hybrids. Flocculation of the finest material is of key
704 importance.
- 705 • Medium silt to fine-grained sandy contourites (20 to 200 microns) show a
706 distinctive contourite depositional trend towards better sorting and coarse-tail
707 skew. The weaker currents deposit material directly from suspended load (limited
708 by current capacity), and then, as current velocity increases, more of the finest
709 fraction remains in suspension, and increased winnowing and saltation becomes
710 more important.
- 711 • Medium to coarse sandy contourites (200-1200 microns) show a trend towards
712 poorer sorting. They result from the action of dominant bedload transport,

713 extensive winnowing, and only intermittent bedload movement of the coarsest
714 fraction at high current speeds.

715 • The nature of sediment supply to the bottom current (pelagic, hemipelagic,
716 bottom-current erosion, shelf-slope spillover and downslope turbidity currents) is
717 of key importance for all contourite facies.

718 • Porosity-depth relationships from the four Cadiz sites show a relatively high
719 initial porosity for both sand and mud facies (50-60%), although these values are
720 lower than 'normal' deep-water muds and sands, perhaps due to the persistent
721 bottom current activity.

722 • Porosity shows a decrease with depth to around 35-40% near 500 m burial depth.
723 According to the exponential models of porosity with depth, contourite porosity
724 should 10-17% for sands and 18-24% for muds at 2500 m burial depth.

725 • Similar porosity-depth trends are present in the Eirik, Newfoundland, Gardar and
726 Canterbury Slope drifts, although the surface sediments show 10-20% higher
727 primary porosity where the contourites are dominantly bioclastic in composition.

728 • All sites reveal anomalies and breaks in the porosity-depth trends, linked to the
729 interbedding of sandy and muddy facies, compositional variation (carbonate vs
730 siliciclastic), and the presence of widespread hiatuses in the sediment record.
731 Over-pressure and higher than normal porosities are common. Differential
732 cementation begins below a few hundred metres burial depth.

733 • These results give good insight into the likely reservoir characteristics of
734 contourites, for both conventional and unconventional reservoirs. They are
735 comparable with those of existing contourite fields, although most of these are
736 mixed turbidite-contourite systems. We now need a deliberate search for the
737 contourite play in the subsurface.

738

739 **Acknowledgements**

740 Many people are to thank for the collection and release of the data used in this
741 study. In particular, we thank the captain, officers and crew, and the scientific and
742 technical shipboard parties of the different IODP expeditions utilised. We each thank
743 our respective institutes for their ongoing support. Xiaohang Yu acknowledges
744 financial support from the National Natural Science Foundation of China (No.
745 41976067).

746 **References**

- 747 Allison, E. & Ledbetter, M. T. 1982. Timing of bottom-water scour recorded by
748 sedimentological parameters in the South Australian Basin. *Marine Geology*,
749 46, 131-147.
- 750 Alonso, B., Ercilla, G., Casas, D., Stow, D. A. V., Rodríguez-Tovar, F. J., Dorador, J.
751 & Hernández-Molina, F.-J. 2016. Contourite vs gravity-flow deposits of the
752 Pleistocene Faro Drift (Gulf of Cadiz): Sedimentological and mineralogical
753 approaches. *Marine Geology*, 377, 77-94.
- 754 Athy, L. F. 1930. Density, porosity and compaction of sedimentary rocks. *AAPG*
755 *Bulletin*, 14, 1-24.
- 756 ASTM International, 1990. Standard method for laboratory determination of water
757 (moisture) content of soil and rock (Standard D2216-90). *In Annual Book of*
758 *ASTM Standards for Soil and Rock* (Vol. 04.08): Philadelphia (Am. Soc.
759 Testing Mater.).
- 760 Bein, A. & Sofer, Z. 1987. Origin of oils in Helez region, Israel--implications for
761 exploration in the eastern Mediterranean. *AAPG Bulletin*, 71, 65-75.
- 762 Bein, A. & Weiler, Y. 1976. The Cretaceous Talme Yafe Formation: a contour current
763 shaped sedimentary prism of calcareous detritus at the continental margin of
764 the Arabian Craton. *Sedimentology*, 23, 511-532.
- 765 Benayad, S., Park, Y.-S., Chaouchi, R. & Kherfi, N. 2013. Unconventional resources
766 in Algeria: appraisal result from the Hamra Quartzite reservoir. *Geosciences*
767 *Journal*, 17, 313-327.
- 768 Blatt, H. 1992. *Sedimentary petrology. 2nd edition*, New York.
- 769 Blott, S. J. & Pye, K. 2001. GRADISTAT: a grain size distribution and statistics
770 package for the analysis of unconsolidated sediments. *Earth surface processes*
771 *and Landforms*, 26, 1237-1248.
- 772 Boggs, S. 2009. *Petrology of sedimentary rocks, second edition*, New York.
- 773 Brackenridge, R. E., Stow, D. A. V., Hernández-Molina, F. J., Jones, C., Mena, A.,
774 Alejo, I., Ducassou, E., Llave, E., Ercilla, G. & A Nombela, M. 2018. Textural
775 characteristics and facies of sand-rich contourite depositional systems.
776 *Sedimentology*, 65, 2223-2252.

- 777 Bridge, J. & Demicco, R. 2008. *Earth surface processes, landforms and sediment*
778 *deposits*, Cambridge University Press.
- 779 Bruna, P.-O., Guglielmi, Y., Lamarche, J., Floquet, M., Fournier, F., Sizun, J.-P.,
780 Gallois, A., Marié, L., Bertrand, C. & Hollender, F. 2013. Porosity gain and
781 loss in unconventional reservoirs: Example of rock typing in Lower
782 Cretaceous hemipelagic limestones, SE France (Provence). *Marine and*
783 *Petroleum Geology*, 48, 186-205.
- 784 Brunner, C. A. 1984. Evidence for increased volume transport of the Florida Current
785 in the Pliocene and Pleistocene. *Marine Geology*, 54, 223-235.
- 786 Buitrago, J., García, C., Cajebread-Brow, J., Jiménez, A. & Martínez del Olmo, W.
787 2001. *Contouritas: un excelente almacén casi desconocido (Golfo de Cádiz,*
788 *SO de España)*. 1er Congreso Técnico Exploración y producción
789 REPSOL-YPF, 2001 Madrid. 24-27.
- 790 Busch, W. 1989. Patterns of Sediment Compaction at Ocean Drilling Program Sites
791 645, 646, and 647, Baffin Bay and Labrador Sea. *Proceedings of the Ocean*
792 *Drilling Program, scientific results, ODP, Leg 105, Baffin Bay and Labrador*
793 *Sea*, 781-790.
- 794 Capella, W., Hernández-Molina, F. J., Flecker, R., Hilgen, F. J., Hssain, M.,
795 Kouwenhoven, T. J., van Oorschot, M., Sierro, F. J., Stow, D. A. V.,
796 Trabucho-Alexandre, J., Tulbure, M. A., de Weger, W., Yousfi, M. Z. &
797 Krijgsman, W. 2017. Sandy contourite drift in the late Miocene Rifian
798 Corridor (Morocco): Reconstruction of depositional environments in a
799 foreland-basin seaway. *Sedimentary Geology*, 355, 31-57.
- 800 Channell, J. E. T., Kanamatsu, T., Sato, T., Stein, R., Alvarez Zarikian, C. A., Malone,
801 M. J. & the Expedition 339 Scientists. 2006. *Proceedings of the Integrated*
802 *Ocean Drilling Program, Volume 303/306. College Station TX* (Integrated
803 Ocean Drilling Program Management International, Inc.).
- 804 Chen, H., Xie, X., Van Rooij, D., Vandorpe, T., Su, M., & Wang, D. (2014).
805 Depositional characteristics and processes of alongslope currents related to a
806 seamount on the northwestern margin of the Northwest Sub-Basin, South
807 China Sea. *Marine Geology*, 355, 36-53.
- 808 Chilingar, G. V. 1964. Relationship Between Porosity, Permeability, and Grain-Size
809 Distribution of Sands and Sandstones. *Developments in Sedimentology*, 1,
810 71-75.
- 811 Cooper, M. C. 1998. The use of digital image analysis in the study of laminated
812 sediments. *Journal of Paleolimnology*, 19, 33-40.
- 813 Faugères, J.-C. & Mulder, T. 2011. Contour Currents and Contourite Drifts. In:
814 HüNeke, H. & Mulder, T. (eds.) *Developments in Sedimentology*. Elsevier.
- 815 Faugères, J.-C. & Stow, D. A. V. 1993. Bottom-current-controlled sedimentation: a
816 synthesis of the contourite problem. *Sedimentary Geology*, 82, 287-297.
- 817 Folk, R. L. & Robles, R. 1964. Carbonate sands of isla perez, alacran reef complex,
818 Yucatan. *The Journal of Geology*, 72, 255-292.
- 819 Folk, R. L. & Ward, W. C. 1957. Brazos River bar [Texas]; a study in the significance
820 of grain size parameters. *Journal of Sedimentary Research*, 27, 3-26.

- 821 Fonnesu, M., Palermo, D., Galbiati, M., Marchesini, M., Bonamini, E. & Bendias, D.
822 2020. A new world-class deep-water play-type, deposited by the
823 syndepositional interaction of turbidity flows and bottom currents: The giant
824 Eocene Coral Field in northern Mozambique. *Marine and Petroleum Geology*,
825 111, 179-201.
- 826 Friedman, G. M., Sanders, J. E., & Kopaska-Merkel, D. C. (1992). *Principles of*
827 *sedimentary deposits: stratigraphy and sedimentology*. Macmillan College.
- 828 Fulthorpe, C. S., Hoyanagi, K., Blum, P. & the Expedition 317 Scientists. 2011.
829 *Proceedings of the Integrated Ocean Drilling Program, Volume 317*. Tokyo
830 (Integrated Ocean Drilling Program Management International, Inc.).
- 831 Gluyas, J. & Swarbrick, R. 2004. *Petroleum Geoscience*. Blackweel Science Ltd:
832 Oxford.
- 833 Gong, C., Wang, Y., Zheng, R., Hernández-Molina, F. J., Li, Y., Stow, D. A. V., Xu,
834 Q. & Brackenridge, R. E. 2016. Middle Miocene reworked turbidites in the
835 Baiyun Sag of the Pearl River Mouth Basin, northern South China Sea margin:
836 processes, genesis, and implications. *Journal of Asian Earth Sciences*, 128,
837 116-129.
- 838 Gonthier, E. G., Faugères, J.-C. & Stow, D. A. V. 1984. Contourite facies of the Faro
839 Drift, Gulf of Cadiz. *Geological Society, London, Special Publications*, 15,
840 275-292.
- 841 Haris, A., Seno, B., Riyanto, A. & Bachtiar, A. 2017. Integrated Approach for
842 Characterizing Unconventional Reservoir Shale Hydrocarbon: Case Study of
843 North Sumatra Basin. *IOP Conference Series: Earth Environmental Science*,
844 62, 12-23.
- 845 Hernandez-Molina, F. J., Llave, E., Preu, B., Ercilla, G., Fontan, A., Bruno, M., Serra,
846 N., Gomiz, J. J., Brackenridge, R. E. & Sierro, F. J. 2014. Contourite
847 processes associated with the Mediterranean Outflow Water after its exit from
848 the Strait of Gibraltar: Global and conceptual implications. *Geology*, 42,
849 227-230.
- 850 Hernández-Molina, F. J., Sierro, F. J., Llave, E., Roque, C., Stow, D. A. V., Williams,
851 T., Lofi, J., Van der Schee, M., Arnáiz, A., Ledesma, S., Rosales, C.,
852 Rodríguez-Tovar, F. J., Pardo-Igúzquiza, E. & Brackenridge, R. E. 2016a.
853 Evolution of the gulf of Cadiz margin and southwest Portugal contourite
854 depositional system: Tectonic, sedimentary and paleoceanographic
855 implications from IODP expedition 339. *Marine Geology*, 377, 7-39.
- 856 Hernández-Molina, F. J., Wåhlin, A., Bruno, M., Ercilla, G., Llave, E., Serra, N.,
857 Rosón, G., Puig, P., Rebesco, M., Van Rooij, D., Roque, D., González-Pola,
858 C., Sánchez, F., Gómez, M., Preu, B., Schwenk, T., Hanebuth, T. J. J.,
859 Sánchez Leal, R. F., García-Lafuente, J., Brackenridge, R. E., Juan, C., Stow,
860 D. A. V. & Sánchez-González, J. M. 2016b. Oceanographic processes and
861 morphosedimentary products along the Iberian margins: A new
862 multidisciplinary approach. *Marine Geology*, 378, 127-156.
- 863 Hollister, C. D. & Heezen, B. C. 1972. *Geologic effects of ocean bottom currents:*
864 *Western North Atlantic*, New York, Gordon and Breach Science Publications.

- 865 Huang, Y., Yao, G., Zhou, F. & Wang, T. 2017. Impact factors on reservoir quality of
866 clastic Huangliu formation in overpressure diapir zone, Yinggehai Basin,
867 China. *Journal of Petroleum Science Engineering*, 154, 322-336.
- 868 Intawong, A., Hodgson, N., Rodriguez, K. & Hargreaves, P. 2019. Oil prospects in
869 the Mozambique Channel: where incipient subduction meets passive margin.
870 *First Break*, 37, 75-81.
- 871 Jansa, L. F. & Urrea, V. H. N. 1990. Geology and Diagenetic History of
872 Overpressured Sandstone Reservoirs, Venture Gas Field, Offshore Nova
873 Scotia, Canada (1). *AAPG Bulletin*, 74, 1640-1658.
- 874 Ledbetter, M. T. & Ellwood, B. B. 1980. Spatial and temporal changes in
875 bottom-water velocity and direction from analysis of particle size and
876 alignment in deep-sea sediment. *Marine Geology*, 38, 245-261.
- 877 Leeder, M. R. 1999. *Sedimentology and sedimentary basins: from turbulence to*
878 *tectonics*, Oxford, Blackwell.
- 879 Li, Y., Wang, X., Wu, B., Li, G. & Wang, D. 2016. Sedimentary facies of marine
880 shale gas formations in Southern China: The Lower Silurian Longmaxi
881 Formation in the southern Sichuan Basin. *Journal of Earth Science*, 27,
882 807-822.
- 883 Lüdmann, T., Betzler, C., Eberli, G. P., Reolid, J., Reijmer, J. J., Sloss, C. R., Bialik,
884 O. M., Alvarez-Zarikian, C. A., Alonso-García, M. & Blättler, C. L. 2018.
885 Carbonate delta drift: A new sediment drift type. *Marine Geology*, 401,
886 98-111.
- 887 Lüdmann, T., Kalvelage, C., Betzler, C., Fürstenau, J. & Hübscher, C. 2013. The
888 Maldives, a giant isolated carbonate platform dominated by bottom currents.
889 *Marine and Petroleum Geology*, 43, 326-340.
- 890 Mahmood, M. F., Ahmad, Z. & Ehsan, M. 2018. Total organic carbon content and
891 total porosity estimation in unconventional resource play using integrated
892 approach through seismic inversion and well logs analysis within the Talhar
893 Shale, Pakistan. *Journal of Natural Gas Science and Engineering*, 52, 13-24.
- 894 Maldonado, A., Somoza, L. s. & Pallarés, L. 1999. The Betic orogen and the Iberian–
895 African boundary in the Gulf of Cadiz: geological evolution (central North
896 Atlantic). *Marine Geology*, 155, 9-43.
- 897 Martins, L. R. 1965. Significance of skewness and kurtosis in environmental
898 interpretation. *Journal of Sedimentary Research*, 35, 768-770.
- 899 Martins, L. R. 2003. Recent sediments and grain-size analysis. *Gravel*, 1, 90-105.
- 900 Mason, C. C. & Folk, R. L. 1958. Differentiation of Beach, Dune, and Aeolian Flat
901 Environments by Size Analysis, Mustang Island, Texas. *Journal of*
902 *Sedimentary Research*, Vol. 28, 211-226.
- 903 Masson, D. G., Plets, R. M. K., Huvenne, V. A. I., Wynn, R. B. & Bett, B. J. 2010.
904 Sedimentology and depositional history of Holocene sandy contourites on the
905 lower slope of the Faroe–Shetland Channel, northwest of the UK. *Marine*
906 *Geology*, 268, 85-96.
- 907 McCave, I. 1984. Erosion, transport and deposition of fine-grained marine sediments.
908 *Geological Society, London, Special Publications*, 15, 35-69.

- 909 McCave, I. 2008. Size sorting during transport and deposition of fine sediments:
910 sortable silt and flow speed. *Developments in Sedimentology*, 60, 121-142.
- 911 McCave, I., Bryant, R., Cook, H. & Coughanowr, C. 1986. Evaluation of a
912 laser-diffraction-size analyzer for use with natural sediments. *Journal of*
913 *Sedimentary Research*, 56.
- 914 McCave, I. N., Manighetti, B. & Robinson, S. G. 1995. Sortable silt and fine sediment
915 size/composition slicing: parameters for palaeocurrent speed and
916 palaeoceanography. *Paleoceanography*, 10, 593-610.
- 917 Moraes, M. A. S., Maciel, W. B., Braga, M. S. S. & Viana, A. R. 2007.
918 *Bottom-current reworked Palaeocene-Eocene deep-water reservoirs of the*
919 *Campos Basin, Brazil*, London, Geological Society of London.
- 920 Mulder, T., Hassan, R., Ducassou, E., Zaragosi, S., Gonthier, E., Hanquiez, V.,
921 Marchès, E. & Toucanne, S. 2013. Contourites in the Gulf of Cadiz: a
922 cautionary note on potentially ambiguous indicators of bottom current velocity.
923 *Geo-Marine Letters*, 33, 357-367.
- 924 Mutti, E. & Carminatti, M. 2012. Deep-water sands of the Brazilian offshore basins.
925 *Search Discovery*.
- 926 Mutti, E., Cunha, R. S., Bulhoes, É. M. & Arienti, L. M. 2014. Contourites and
927 Turbidites of the Brazilian Marginal Basins. *AAPG Annual Convention &*
928 *Exhibition*. Houston, USA.
- 929 Nicholson, U. & Stow, D. 2019. Erosion and deposition beneath the Subantarctic
930 Front since the Early Oligocene. *Scientific Reports*, 9, 9296.
- 931 Norris, R. D., Wilson, P. A., Blum, P. & the Expedition 339 Scientists. 2014.
932 *Proceedings of the Integrated Ocean Drilling Program, Volume 342*. College
933 Station TX (Integrated Ocean Drilling Program Management International,
934 Inc.).
- 935 Osborne, M. & Swarbrick, R. 1997. Mechanisms for Generating Overpressure in
936 Sedimentary Basins_ A Reevaluation. *AAPG Bulletin*, 81 (1997), 1032-1041.
- 937 Palermo, D., Galbiati, M., Famiglietti, M., Marchesini, M., Mezzapesa, D. & Fonesu,
938 F. Insights into a new super-giant gas field-sedimentology and reservoir
939 modeling of the Coral Reservoir Complex, Offshore Northern Mozambique.
940 Offshore Technology Conference-Asia, 2014. Offshore Technology
941 Conference.
- 942 Pettingill, H. S. & Weimer, P. 2002. Worldwide deepwater exploration and production:
943 Past, present, and future. *The Leading Edge*, 21, 371-376.
- 944 Pollack, J. M. 1961. Significance of Compositional and Textural Properties of South
945 Canadian River Channel Sands, New Mexico, Texas and Oklahoma. *Journal*
946 *of Sedimentary Research*, Vol. 31, 795-801.
- 947 Rebesco, M. & Camerlenghi, A. 2008. *Contourites*, Amsterdam, Elsevier Science.
- 948 Rebesco, M., Hernández-Molina, F. J., Van Rooij, D. & Wåhlin, A. 2014. Contourites
949 and associated sediments controlled by deep-water circulation processes:
950 State-of-the-art and future considerations. *Marine Geology*, 352, 111-154.
- 951 Rubey, W. W. & Hubbert, M. K. 1959. Role of Fluid Pressure in Mechanics of
952 Overthrust Faulting. *Geological Society of America Bulletin*, 70.

- 953 Rundberg, Y. & Eidvin, T. 2016. Discussion on ‘Late Cenozoic geological evolution
954 of the northern North Sea: development of a Miocene unconformity reshaped
955 by large-scale Pleistocene sand intrusion’ *Journal of the Geological Society*,
956 170, 133–145. *Journal of the Geological Society*, 173, 384-393.
- 957 Sansom, P. 2018. Hybrid turbidite–contourite systems of the Tanzanian margin.
958 *Petroleum Geoscience*, 24, 258-276.
- 959 Scherer, M. 1987. Parameters influencing porosity in sandstones: a model for
960 sandstone porosity prediction. *AAPG bulletin*, 71, 485-491.
- 961 Sclater, J. G. & Christie, P. A. F. 1980. Continental stretching: An explanation of the
962 Post-Mid-Cretaceous subsidence of the central North Sea Basin. *Journal of*
963 *Geophysical Research: Solid Earth*, 85, 3711-3739.
- 964 Selley, R. C. 2000. *Applied sedimentology*, Elsevier.
- 965 Shanmugam, G. 2006. *Deep-water processes and facies models: Implications for*
966 *sandstone petroleum reservoirs*, Elsevier.
- 967 Shanmugam, G. 2012. *New perspectives on deep-water sandstones: Origin,*
968 *recognition, initiation, and reservoir quality (Vol. 9)*. Elsevier.
- 969 Shanmugam, G. 2017. Contourites: Physical oceanography, process sedimentology,
970 and petroleum geology. *Petroleum Exploration and Development*, 44,
971 183-216.
- 972 Stow, D. A. V. 2005. *Sedimentary rocks in the field: A colour guide*, CRC Press.
- 973 Stow, D. A.V., Armishaw, J. E. & Holmes, R. 2002a. Holocene contourite sand sheet
974 on the Barra Fan slope, NW Hebridean margin. *Geological Society, London,*
975 *Memoirs*, 22, 99-119.
- 976 Stow, D. A. V., Brackenridge, R. & Hernandez-Molina, F. J. Contourite sheet sands:
977 new deepwater exploration target. American Association of Petroleum
978 Geologists Annual Conference, 2011 Houston.
- 979 Stow, D. A. V., Faugères, J.-C., Howe, J. A., Pudsey, C. J. & Viana, A. R. 2002b.
980 Bottom currents, contourites and deep-sea sediment drifts: current
981 state-of-the-art. *Geological Society, London, Memoirs*, 22, 7-20.
- 982 Stow, D. A. V. & Faugères, J. C. 2008. Contourite Facies and the Facies Model. *In:*
983 *Rebesco, M. & Camerlenghi, A. (eds.) Developments in Sedimentology.*
984 Elsevier.
- 985 Stow, D. A. V., Hernández-Molina, F., Zarikian, C. & Expedition Shipboard
986 Scientists. 2014. New Advances in the Contourite Paradigm: IODP Expedition
987 339, Gulf of Cadiz. *2nd Deep-Water Circulation Congress*. Ghent, Belgium.
- 988 Stow, D. A. V., Hernández-Molina, F. J., Alvarez Zarikian, C. A. & Expedition 339
989 Scientists. 2013a. *Proceedings of the Integrated Ocean Drilling Program,*
990 *Volume 339. Tokyo* (Integrated Ocean Drilling Program Management
991 International, Inc.).
- 992 Stow, D. A. V., Hernández-Molina, F. J., Llave, E., Bruno, M., García, M., Díaz del
993 Rio, V., Somoza, L. & Brackenridge, R. E. 2013b. The Cadiz Contourite
994 Channel: Sandy contourites, bedforms and dynamic current interaction.
995 *Marine Geology*, 343, 99-114.

- 996 Stow, D. A. V., & Holbrook, J. A. (1984). North Atlantic contourites: an
997 overview. *Geological Society, London, Special Publications*, 15(1), 245-256.
- 998 Stow, D. A. V., Hunter, S., Wilkinson, D. & Hernández-Molina, F. J. 2008. The
999 nature of contourite deposition. In: Rebesco, M. & Camerlenghi, A. (eds.)
1000 *Developments in sedimentology*.
- 1001 Stow, D. A. V. & Mayall, M. 2000. Deep-water sedimentary systems: New models
1002 for the 21st century. *Marine and Petroleum Geology*, 17, 125-135.
- 1003 Stricker, S. & Jones, S. J. 2018. Enhanced porosity preservation by pore fluid
1004 overpressure and chlorite grain coatings in the Triassic Skagerrak, Central
1005 Graben, North Sea, UK. *Geological Society London Special Publications*, 435,
1006 321-341.
- 1007 Viana, A. R. 2008. Economic Relevance of Contourites. In: Rebesco, M. &
1008 Camerlenghi, A. (eds.) *Developments in Sedimentology*. Elsevier.
- 1009 Viana, A. R., Almeida JR, W., Nunes, M. C. V. & Bulhoese, M. 2007. *The Economic*
1010 *Importance of Contourites*, London, Geological Society of London.
- 1011 Viana, A. R., Faugeres, J. C. & Stow, D. A. V. 1998. Bottom-current-controlled sand
1012 deposits - a review of modern shallow- to deep-water environments.
1013 *Sedimentary Geology*, 115, 53-80.
- 1014 Wangen, M. 2010. Generation of overpressure by cementation of pore space in
1015 sedimentary rocks. *Geophysical Journal International*, 143, 608-620.
- 1016 Waples, D. W. & Couples, G. D. 1998. Some thoughts on porosity reduction -- rock
1017 mechanics, overpressure and fluid flow. *Geological Society London Special*
1018 *Publications*, 141, 73-81.
- 1019 Wen, Z., Xu, H., Wang, Z., He, Z., Song, C., Chen, X. & Wang, Y. 2016.
1020 Classification and hydrocarbon distribution of passive continental margin
1021 basins. *Petroleum Exploration and Development*, 43, 740-750.
- 1022 Wentworth, C. K. 1922. A scale of grade and class terms for clastic sediments. *The*
1023 *journal of geology*, 30, 377-392.
- 1024 Yang, B. 2018. Geological characteristics and reservoir properties in the
1025 unconventional Montney Formation, southwestern Alberta, Canada.
1026 *Geosciences Journal*, 22, 313-325.
- 1027 Zhu, G., Gu, L., Su, J., Dai, J., Ding, W., Zhang, J. & Song, L. 2012. Sedimentary
1028 association of alternated mudstones and tight sandstones in China's oil and gas
1029 bearing basins and its natural gas accumulation. *Journal of Asian Earth*
1030 *Sciences*, 50, 88-104.

Figure Captions

Fig. 1 Morphological map of the Gulf of Cadiz. The yellow circles show the locations of the sites U1386, U1387, U1388 and U1389 of IODP 339, and the green pentagons show the locations of BC04, PC04, PC06 and PC08 of the CONTOURIBER-1 expedition. The red lines mark the principal bottom-currents associated with the Mediterranean Outflow Water. Modified from Hernández-Molina et al. (2006) and Expedition 339 Scientists (2013).

Fig. 2 Summary well logs for IODP 339 sites U1386, U1387, U1388 and U1389 in the Gulf of Cadiz, with schematic representation of the main facies present, and principal hiatuses. mbsf = metres below sea floor.

Fig. 3 Core photographs of the principal contourite, turbidite, debrite and hemipelagite facies recovered IODP 339 sites in the Gulf of Cadiz. Bi-gradational and partial contourite sequences as shown.

Fig. 4 Grain-size parameters cross-plots of over 1000 samples from Gulf of Cadiz contourites. Cores BC05, PC08, PC04 and PC06, after Brackenridge et al (2018); samples from IODP 339 sites U1386, U1387, U1388 and U1389, new for this study. (A) mean grain size versus sorting, (B) mean grain size versus skewness, (C) mean grain size versus kurtosis indicate finest and coarsest sediments have similar kurtosis, (D) sorting versus skewness, (E) kurtosis versus skewness. A-C indicate sites from which samples are derived; D-E indicate grain-size classes

of each sample plotted.

Fig. 5 Porosity-depth profiles for sites U1386, U1387, U1388 and U1389. Because of problems with core recovery of sandy sediments, U1388 has much less data points than the others. Different sites are shown in different colours. The green and yellow lines are estimated trends for mud and sand respectively. These are mostly contourite facies. Below about 400 m at sites U1386 and U1387 (see Figure 2) the succession comprises interbedded contourites, turbidites, debrites and hemipelagites. Blue and red dashed lines show the minor hiatus and major hiatus in U1386, U1387 and U1389 respectively.

Fig. 6 Porosity-depth profiles of Eirik drift (U1305, IODP 303), Gardar drift (U1304, IODP 303), Newfoundland drift (U1410, IODP 342) and Canterbury slope (U1352, IODP 317). Sediments types of Newfoundland drift are showing in different colours.

Fig. 7 Exponential models for porosity-depth profiles of sand (A) and mud (B) contourites, derived from porosity data of U1386, U1387, U1388 and U1389. Predictions are made to likely reservoir depths of 2500m, although the actual porosity data for these sites is between 250-850m depth. The parameters of normal sand and mud are provided after Rubey and Hubbert (1959) and Sclater and Christie (1980). Because of the lack of sand porosity data for U1389, only sand porosity models of U1386, U1387 and U1388 are derived. Due to some anomalous porosity values (i.e. increasing trends) in U1388 and U1389, the exponential curves cannot be derived for these sites.

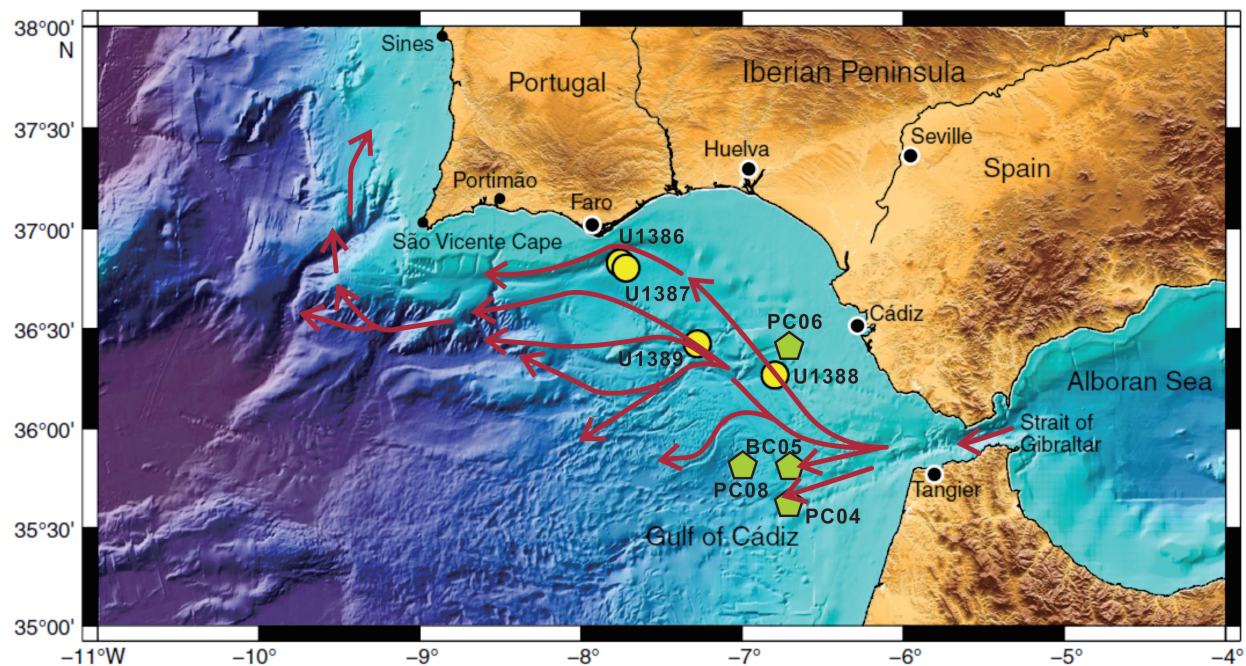
Fig. 8 Summary grain-size cross plots and their interpretation.

- (A) Schematic representation of best-fit trend lines for mean size vs sorting (red), mean size vs skewness (green), and mean size vs skewness (blue). Upper peak values show mean grain size for poorest sorting, most fine-tail skew, and most leptokurtic distribution. Lower peak values show mean grain size for best sorting, most coarse-tail skew, and most platykurtic distribution.
- (B) Schematic representation of best-fit trend line for mean grain size vs sorting (as above), noting grain-size attributes of the three principal facies classes of contourites, and the inferred depositional processes for each. The small curves adjacent to the trend line illustrate the general shape of grain-size distribution curves at different points along the line.

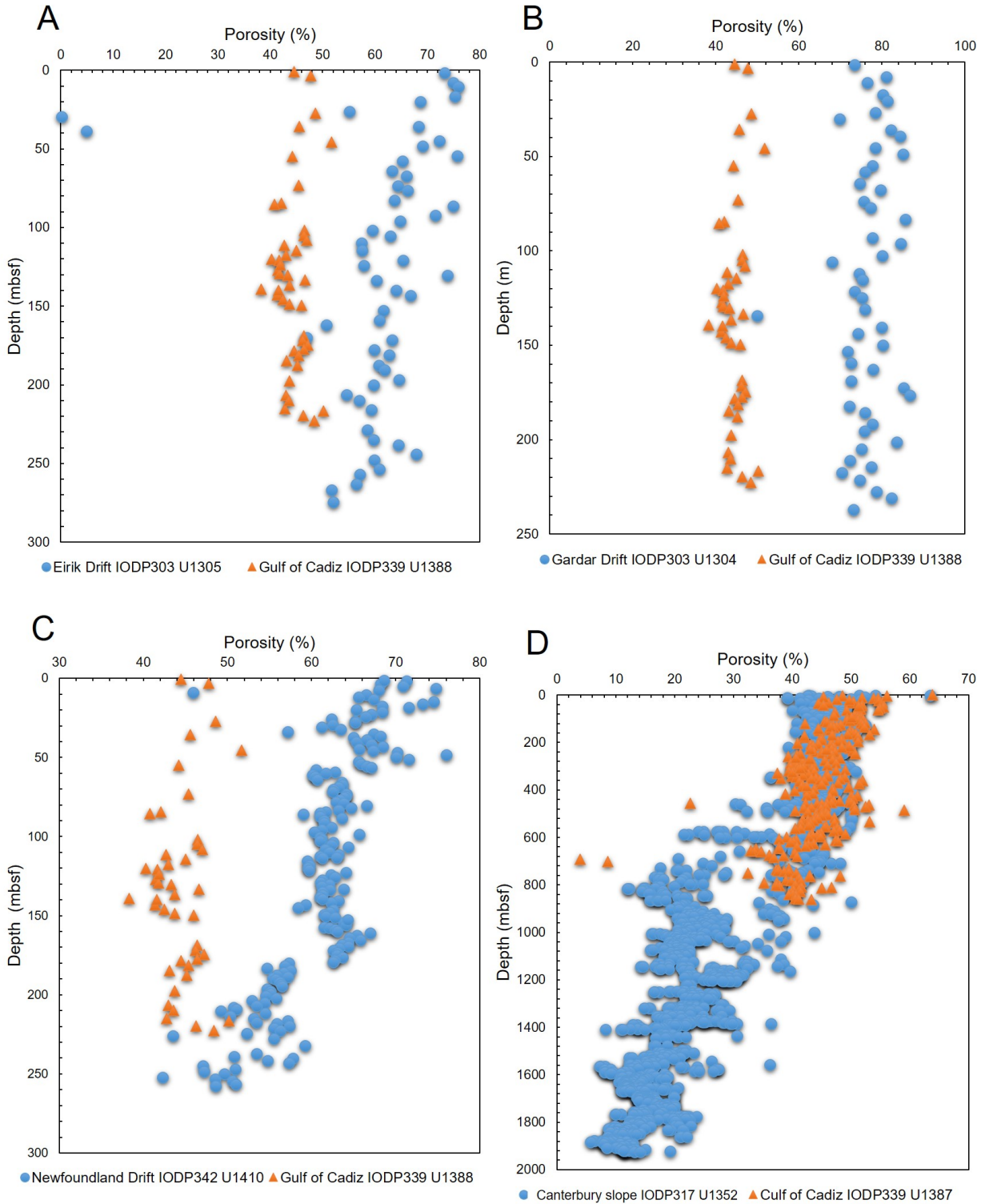
Fig. 9 Abnormal pressure intervals defined by abnormal porosity change trends are shown in the porosity-depth profiles of U1386, U1387, U1388 and U1389, indicating the occurrence of overpressure zones. This is an effective way to prevent porosity decrease during burial and retain high porosity values, at least locally.

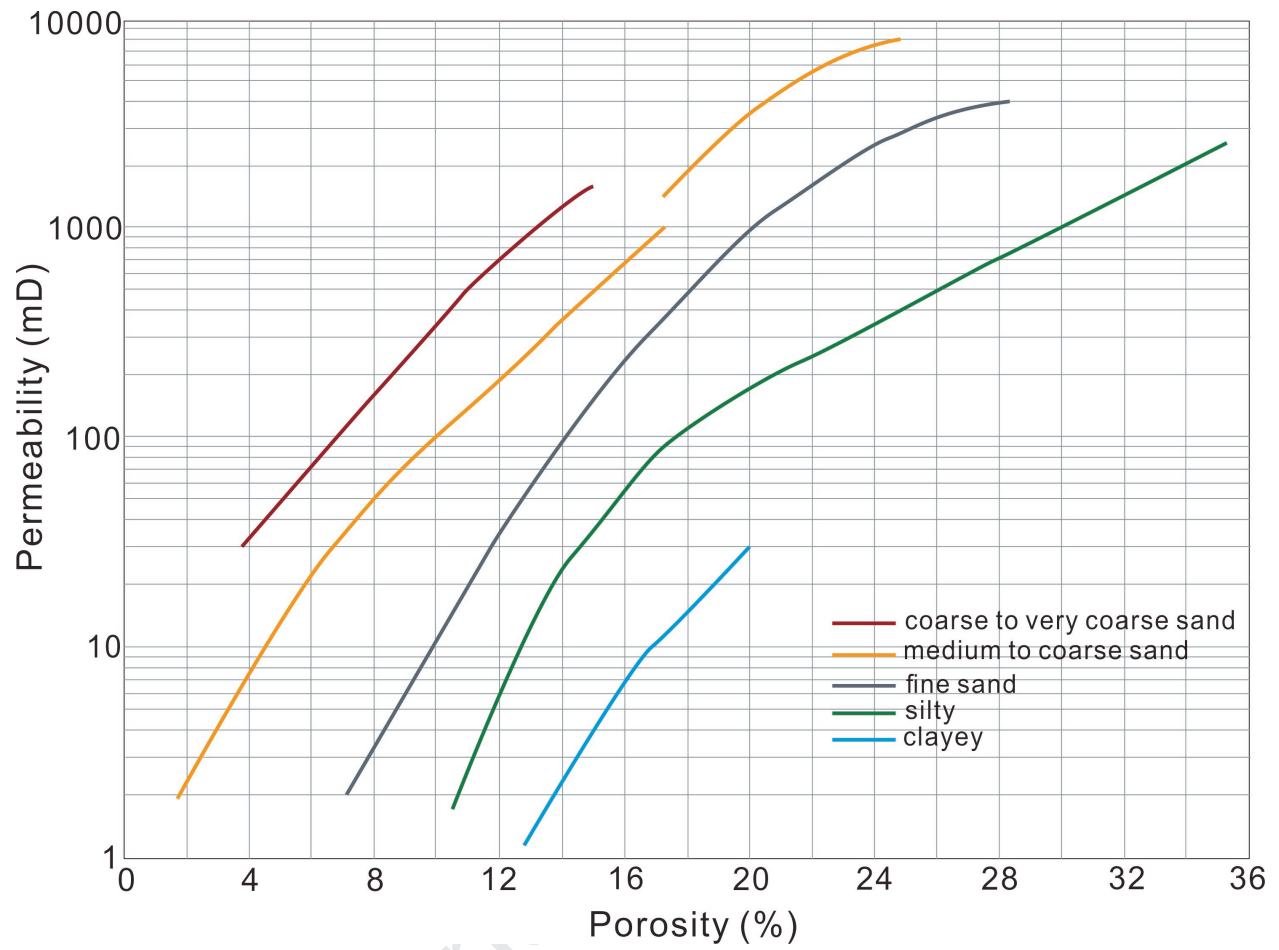
Fig. 10 Comparison of porosity-depth relationship between (A) U1305 (Eirik drift) and U1388 (Gulf of Cadiz); (B) U1304 (Gardar drift) and U1388 (Gulf of Cadiz); (C) U1410 (Newfoundland drift) and U1388 (Gulf of Cadiz); and (D) U1352 (Canterbury slope) and U1387 (Gulf of Cadiz).

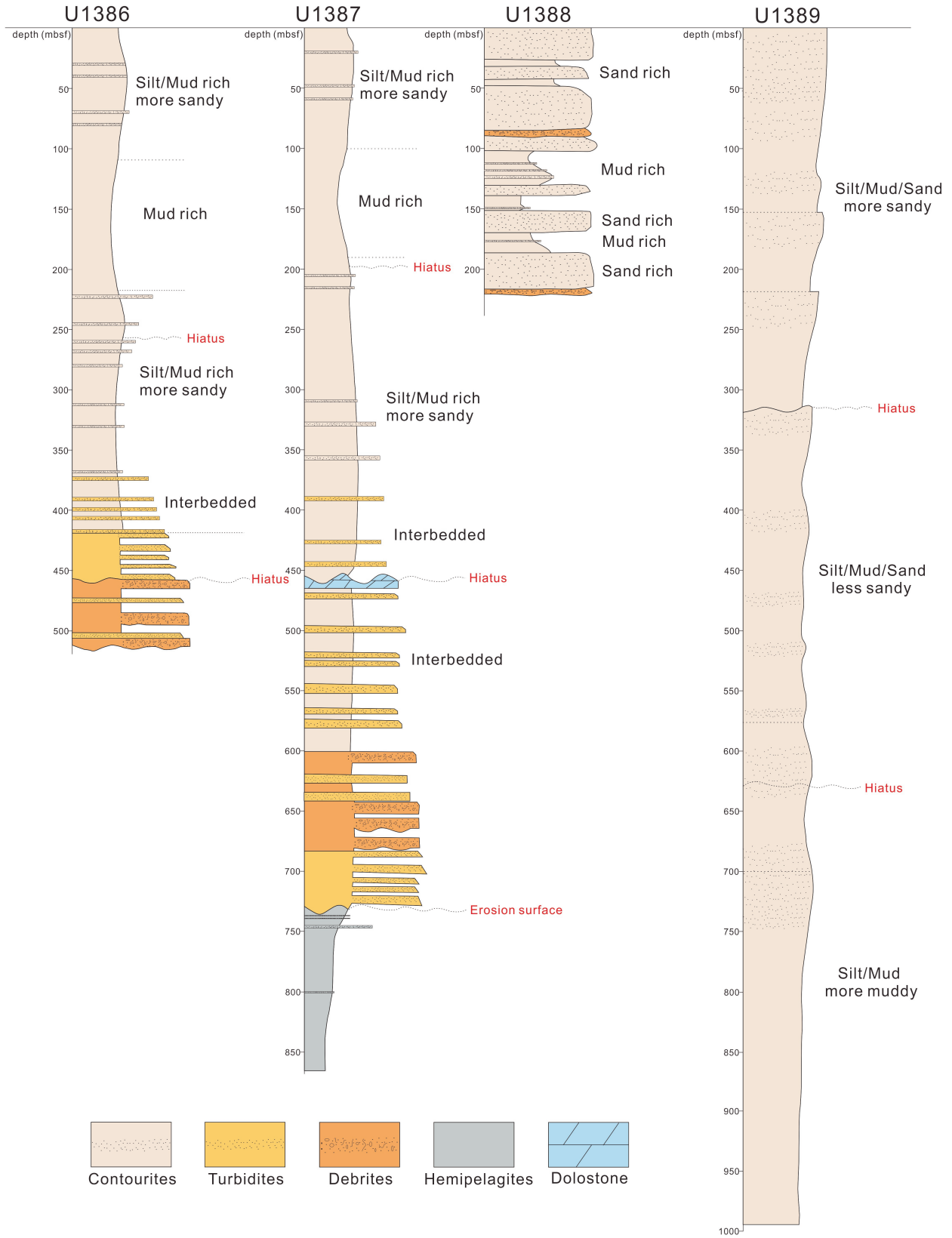
Fig. 11 Typical relationships among permeability, porosity and grain-size, modified from Chilingar (1964). Different colour lines are for different grain-size of sediments. According to Chilingar (1964), coarse to very coarse sand contains more than 50% of 0 ~ -1 phi fraction, medium to coarse sand contains more than 50% of 2 ~ 1 phi fraction, fine sand contains more than 50% of 3 ~ 2 phi fraction, silty (sandstone) contains more than 10% of silt fraction, and clayey (sandstone) contains more than 7% of clay fraction.

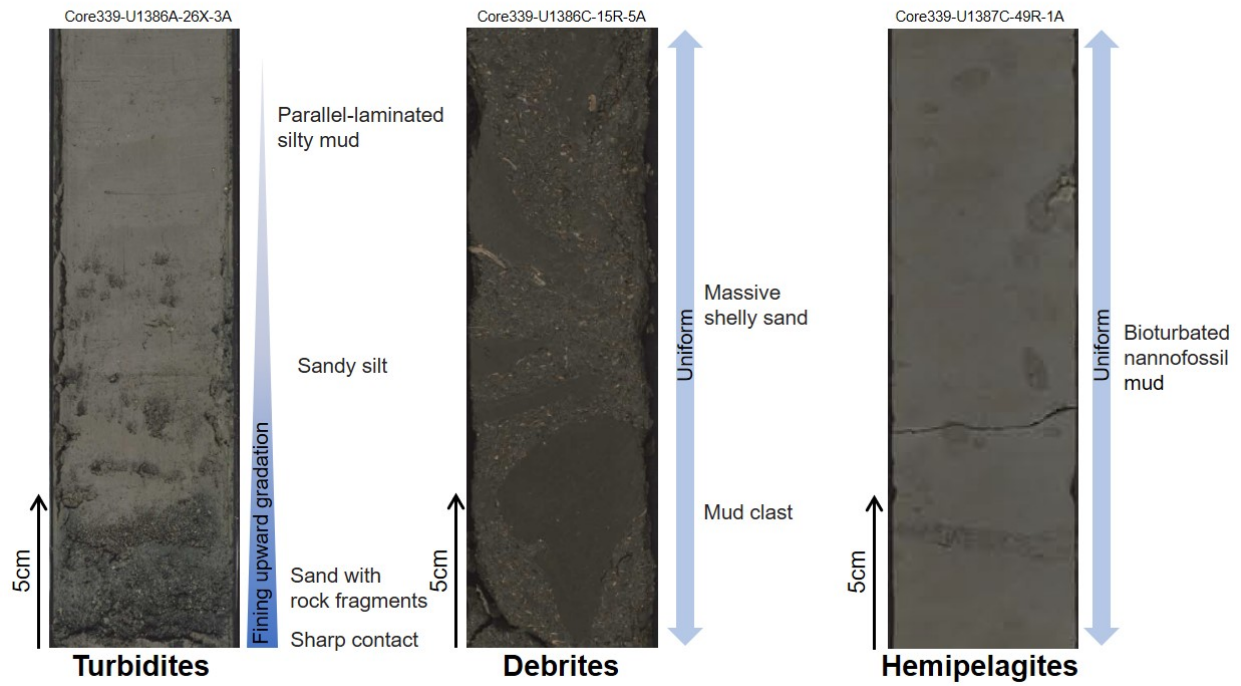
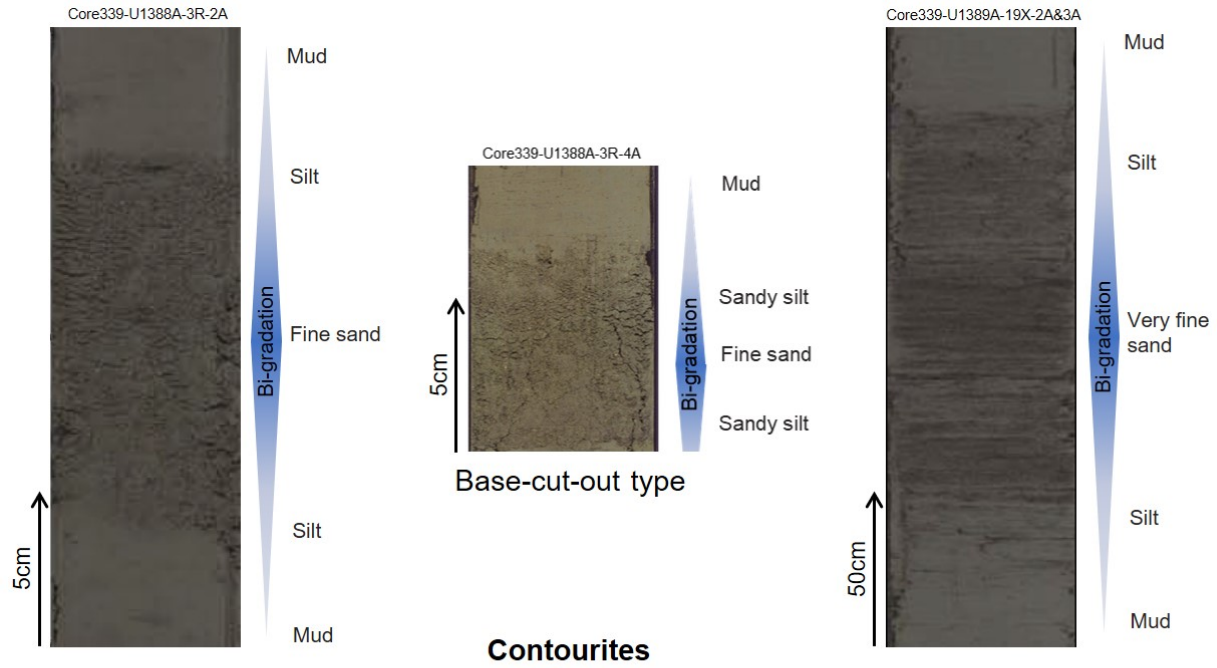


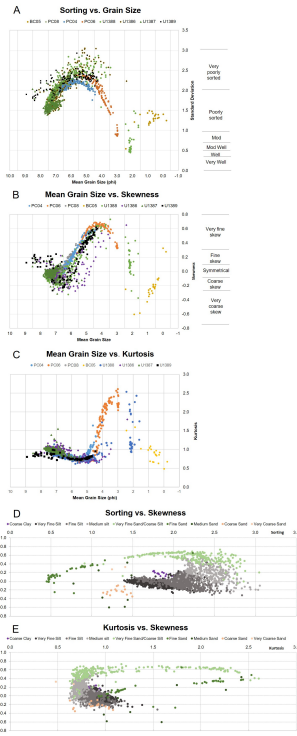
Journal Pre-proof

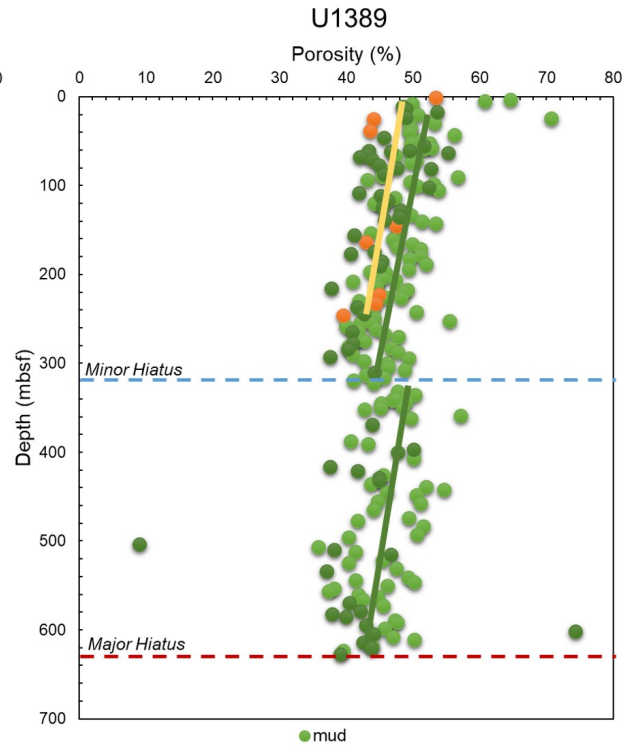
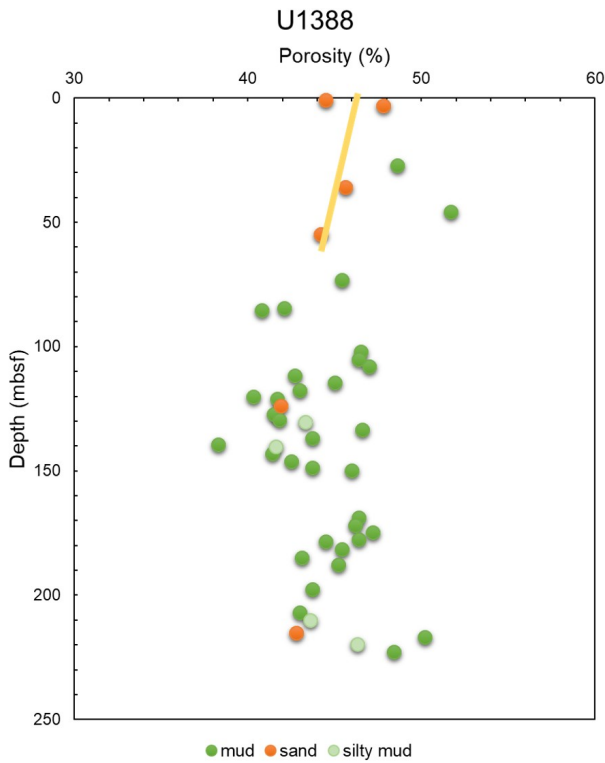
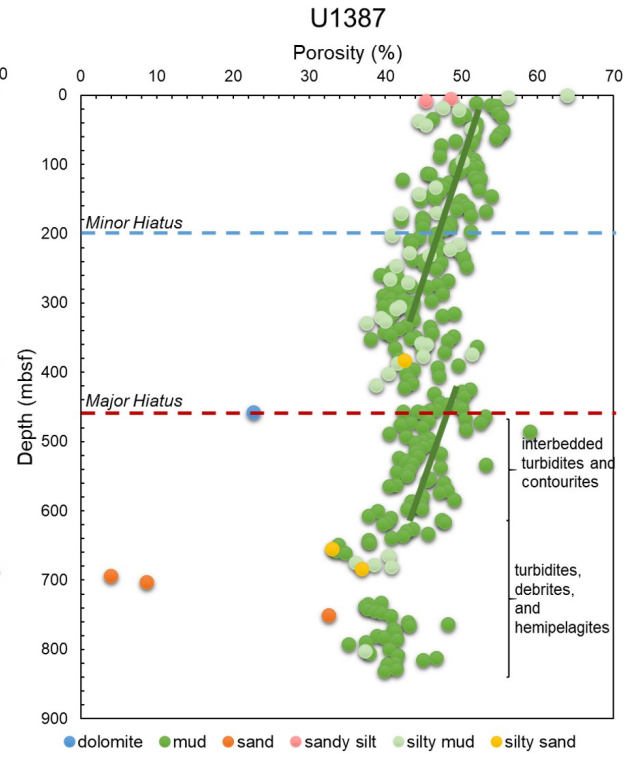
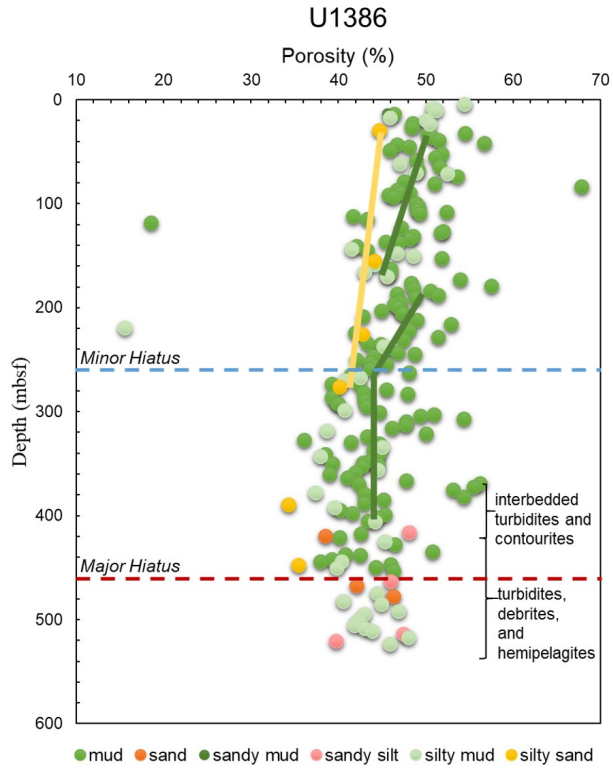




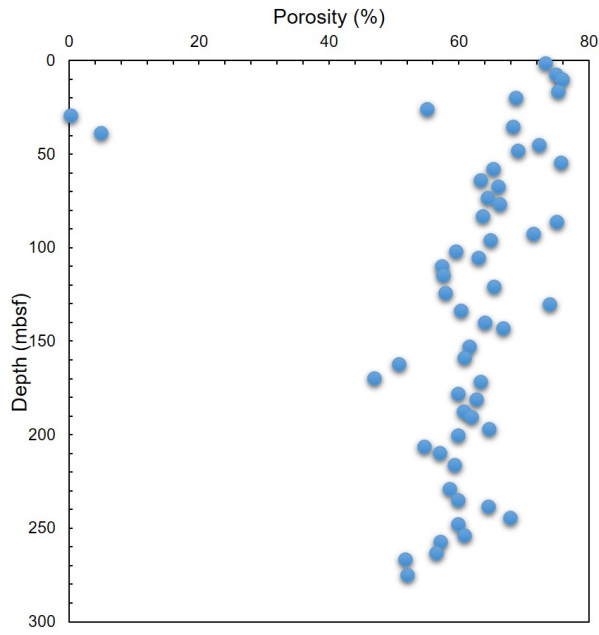




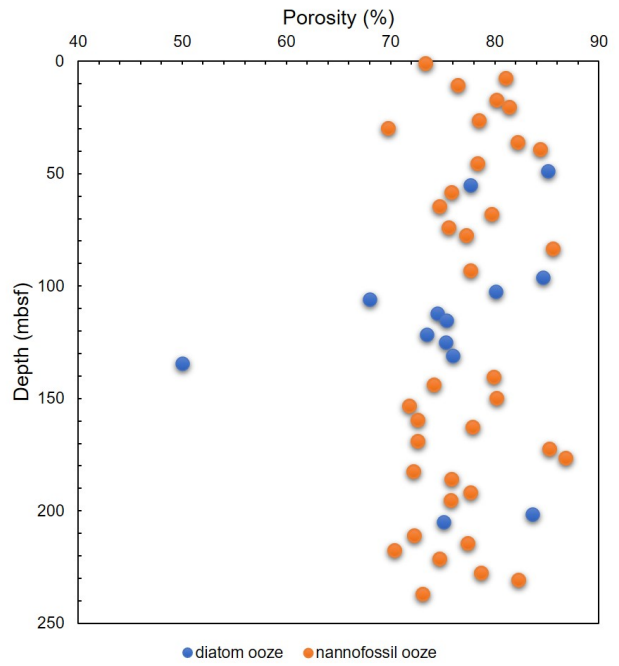




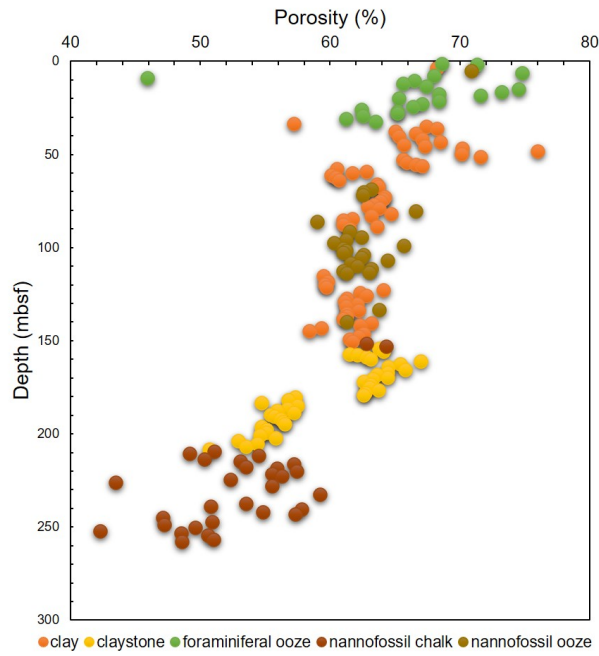
Eirik Drift (U1305, IODP 303)



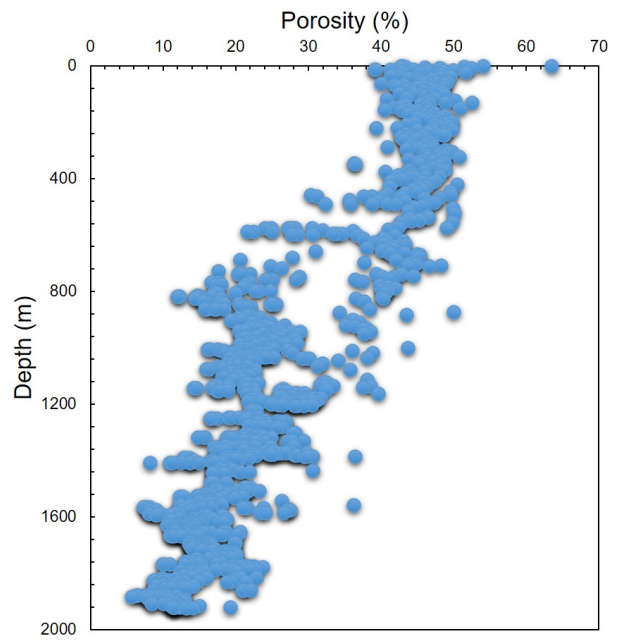
Gardar Drift (U1304, IODP 303)

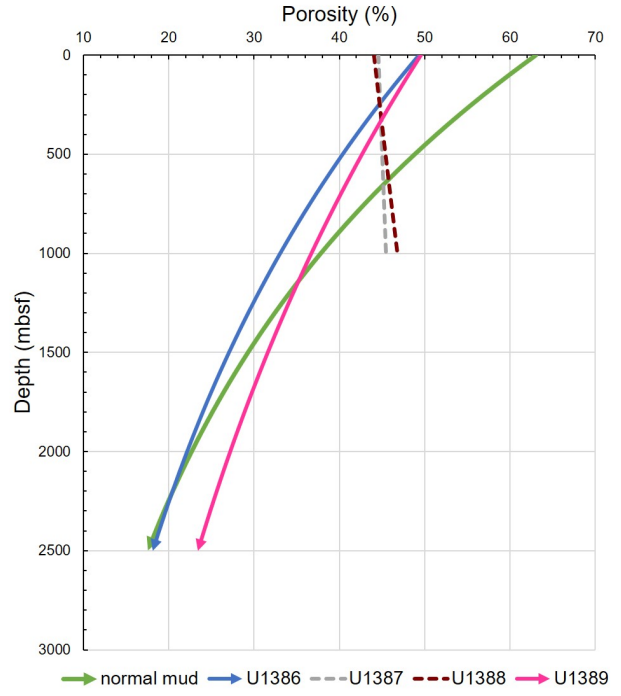
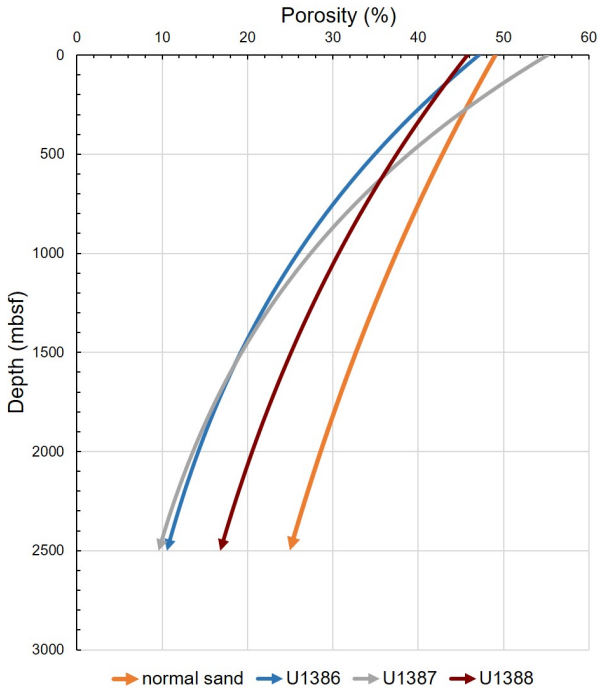


Newfoundland Drift (U1410, IODP 342)



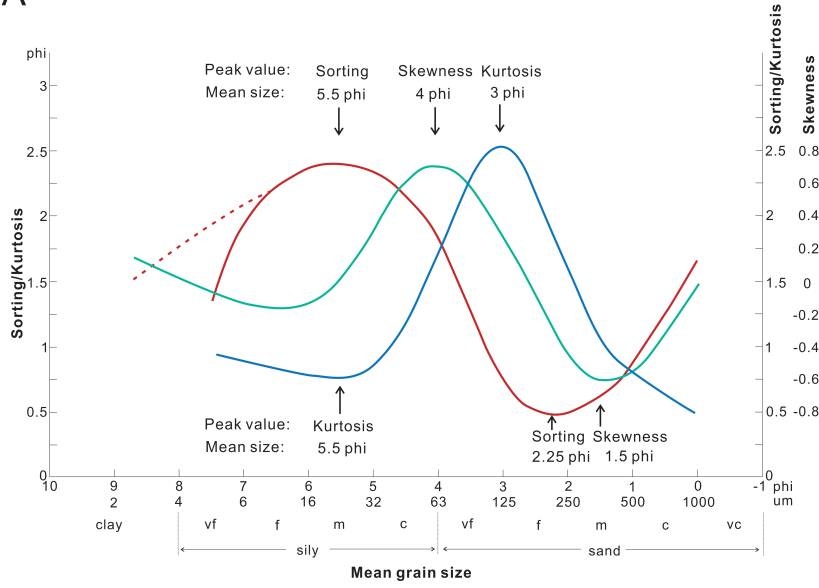
Canterbury Slope (U1352, IODP 317)



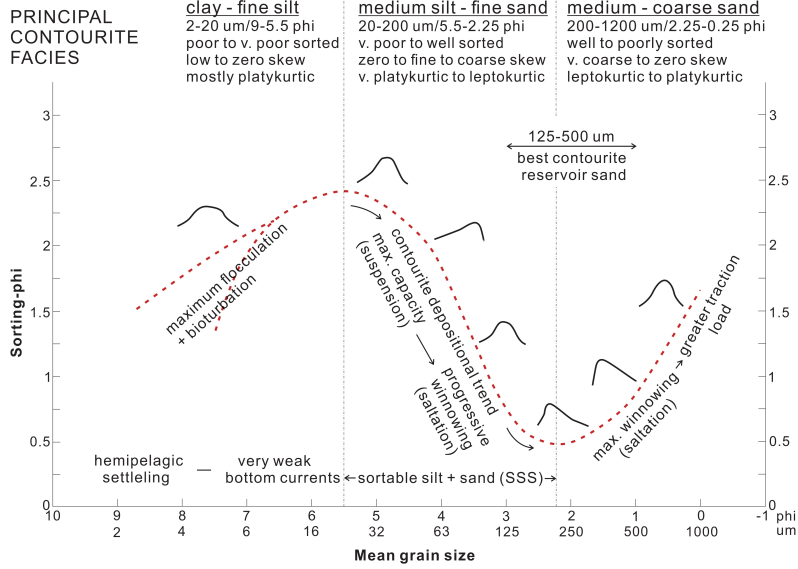


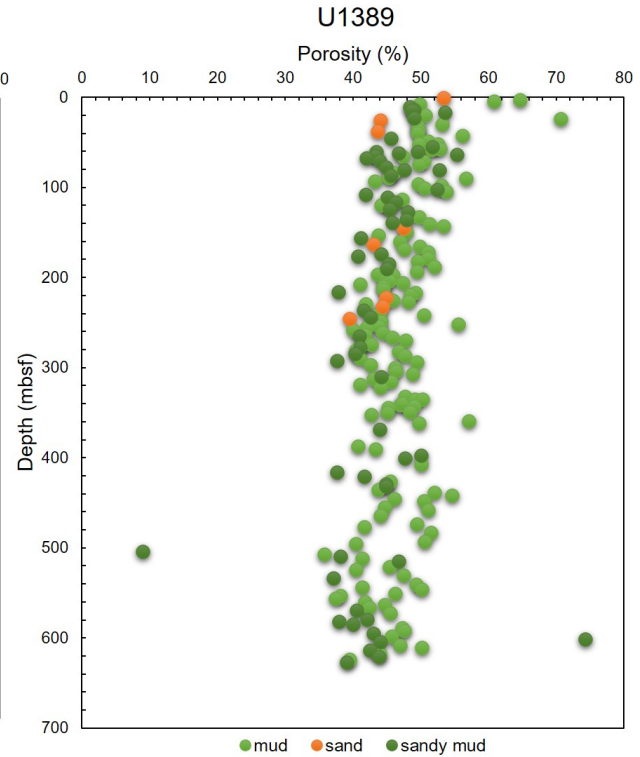
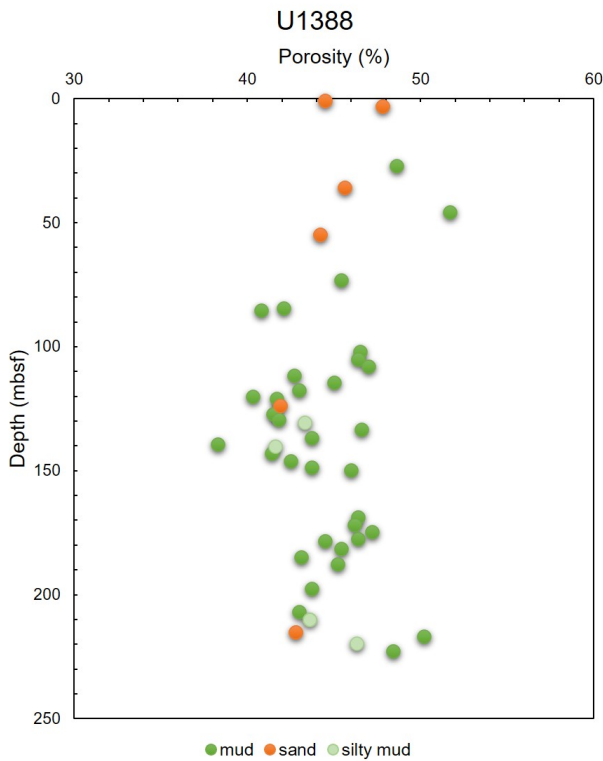
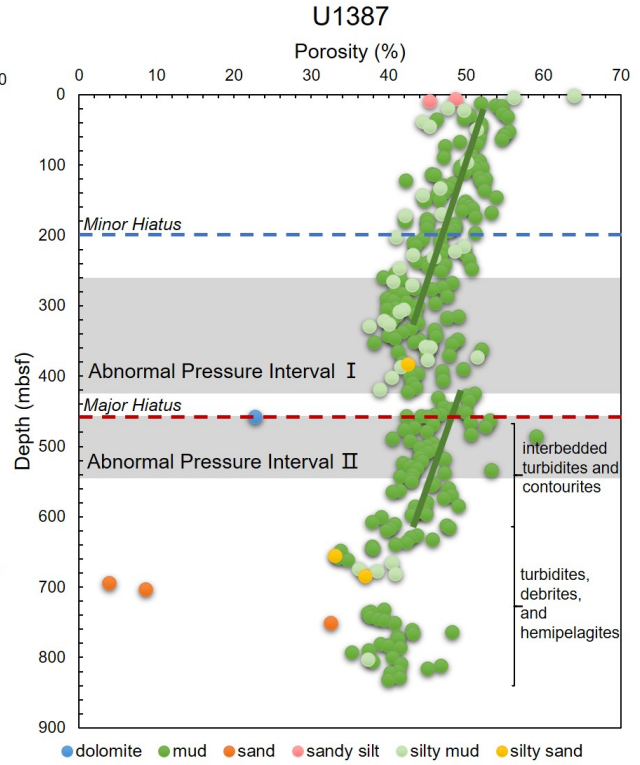
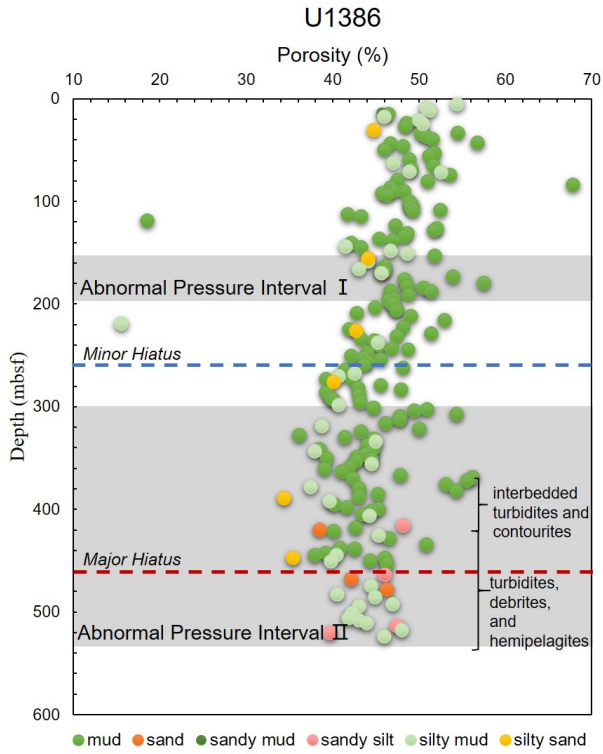
Journal Pre-proof

A



B





Contourite Porosity, Grain Size and Reservoir Characteristics

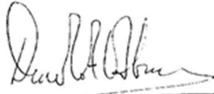
Xiaohang Yu, Dorrik Stow, Zeinab Smillie, Ibimina Esentia, Rachel Brackenridge, Xinong Xie, Shereef Bankole, Emmanuelle Ducassou, Estefania Llave

HIGHLIGHTS

- First publication of comprehensive porosity data for contourites.
- Derivation of exponential models of porosity-depth plots to reservoir depths.
- New understanding of contourite depositional processes from grain-size data.
- Potential reservoir characteristics of contourite systems.

Declaration of Interest statement

We declare that we do not have any commercial or associative interest that represents a conflict of interest in connection with the work submitted.



Prof. Dorrik Stow

Journal Pre-proof